This dissertation has been
microfilmed exactly as received 68-14,801

JOSEPH, Robert Roderick, 1940-
THE LOW TEMPERATURE SPECIFIC HEAT
OF SOME CERIUM AND LANTHANUM LAVES
PHASE COMPOUNDS.

Iowa State University, Ph.D., 1968
Engineering, metallurgy

University Microfilms, Inc., Ann Arbor, Michigan

# THE LOW TEMPERATURE SPECIFIC HEAT OF SOME CERIUM AND LANTHANUM LAVES PHASE COMPOUNDS

by

Robert Roderick Joseph

A Dissertation Submitted to the
Graduate Faculty in Partial Fulfillment of
The Requirements for the Degree of
DOCTOR OF PHILOSOPHY

Major Subject: Metallurgy

Approved:

Signature was redacted for privacy.

In Charge of Major Work

Signature was redacted for privacy.

Head of Major Department

Signature was redacted for privacy.

Dean of Graduate College

Iowa State University
Ames, Iowa

1968

# TABLE OF CONTENTS


| | Page |
|---|---|
| INTRODUCTION | 1 |
| SAMPLE PREPARATION | 11 |
| CALORIMETRY | 22 |
| Apparatus | 22 |
| Temperature Measurement | 26 |
| Heater Current Measurement | 29 |
| Data Acquisition and Reduction | 30 |
| Thermometry | 35 |
| Errors | 38 |
| Magnetic Susceptibility Measurement | 39 |
| RESULTS AND DISCUSSION | 41 |
| $CePt_2$ and $LaPt_2$ | 41 |
| $LaRu_2$ | 51 |
| $CeRu_2$ | 55 |
| SUMMARY | 61 |
| ACKNOWLEDGEMENTS | 64 |
| BIBLIOGRAPHY | 65 |
| APPENDIX | 69 |

# INTRODUCTION

Cerium metal is the only pure metal which undergoes an abrupt change in valence with temperature. It is therefore an interesting material to study because the effect of different valence states on electronic and magnetic properties can be observed. Studies of this valence change should contribute to an increased understanding of the electronic nature of solids.

Cerium metal exists in four allotropic modifications (1). At high temperatures it is body centered cubic ($\delta$) and undergoes a body centered to face centered ($\delta \rightarrow \gamma$) transformation at 1001$^{o}$K. Upon cooling $\gamma$ cerium transforms to the characteristic double close packed structure ($\beta$) of the light rare earths. The transformation is sluggish and shows a large amount of thermal hysteresis. On cooling the transformation temperature is 250$^{o}$K and on heating it is 441$^{o}$K. At lower temperatures another phase ($\alpha$) becomes stable with respect to any untransformed $\gamma$ cerium. $\alpha$-cerium is also face centered cubic but it has a greatly reduced volume (-17 percent) compared to the higher temperature face centered cubic form ($\gamma$). This transformation also exhibits considerable hysteresis. On heating $\alpha$ is stable to 180$^{o}$K but it does not start to form on cooling until the temperature is lowered to below 120$^{o}$K. If $\beta$-Ce transforms to $\alpha$ it only does so below 4$^{o}$K.

Since cerium is known to have one localized 4f electron

it was surmised that the transformation $\gamma \rightarrow \alpha$ was due to the transfer of an electron from the localized 4f shell into the conduction band thus giving the large volume decrease (L. Pauling as quoted by (2) and W. Zachariason as quoted by (3)). It is also possible to force the 4f electron into the conduction band by the application of pressure, 8000 atm at room temperature. The valence of the various allotropes of cerium has been calculated from measured magnetic susceptibility data and atomic radii (4). The values given are 3.06 ± .06 for $\gamma$ cerium and 3.67 ± .09 for $\alpha$ cerium. The transformation of $\gamma$ cerium to $\alpha$ cerium on cooling is never complete at atmospheric pressure because of the formation of $\beta$ cerium. The $\beta$ cerium is stable till at least 4.2°K thus the only way to get samples of pure $\alpha$ cerium is to apply pressure at room temperature and then cool under pressure to form $\alpha$ cerium. The application of pressure causes $\gamma$ and $\alpha$ to become stable with respect to $\beta$ and thus prevents the formation of $\beta$ upon cooling.

Because of the above difficulties in examining pure cerium, it was thought that it might be interesting to look for other techniques for studying the different valence states of cerium. It was observed that the cubic Laves phase $CeRu_2$ became superconducting at 4.9°K (5). Because a large localized magnetic moment prohibits superconductivity, the electrons in $CeRu_2$ must not have much localized 4f character. Therefore in this compound the cerium must be approximately

four valent. Also a plot of the lattice parameters of the compounds R $Ru_2$ (where R stands for a rare earth element) versus atomic number shows an anomaly for the cerium compound. The lattice parameter of $CeRu_2$ is 1.6 per cent smaller than that predicted from an interpolation of the lattice parameters of the other tri-valent lanthanides (6). If all the change in lattice parameter were due to a shrinkage of the cerium atom this would correspond to a volume change of 14.4 per cent contrasted with the 17 per cent change observed for pure cerium. In contrast to $CeRu_2$ the lattice parameter of the cubic Laves phase $CePt_2$ shows no deviation.

To better analyze the behavior of cerium Laves phases the lattice parameter difference between the actual compound and that which would be expected from a plot of the lanthanide compound lattice parameters versus atomic number was determined. This difference was then converted to a volume difference per cerium atom and is given in Table 1 (data from 6,7,8).

Table 1. Interpolated volume minus actual volume of the cerium atom in cerium Laves phases

| Compound | $\Delta V/V_i$ % | Compound | $\Delta V/V_i$ % |
|---|---|---|---|
| $CeMg_2$ | 0 | $CeOs_2$ | 12.5 |
| $CeAl_2$ | 0 | $CeNi_2$ | 13.0 |
| $CePt_2$ | 0 | $CeRu_2$ | 14.4 |
| $CeRh_2$ | 7.8 | $CeCo_2$ | 23.4 |
| $CeIr_2$ | 8.9 | $CeFe_2$ | 27.4 |

$V_i$ = interpolated volume (trivalent Ce)

Based upon the above table one could make the assumption that the valence of cerium increases as the volume difference increases. To see if this approach is reasonable we will examine some of the electrical and magnetic properties of these compounds. $CeAl_2$ (9) and $CeFe_2$ (10) are known to order magnetically and the compound $CePt_2$ was found to order in this study. $CeRu_2$ and $CeCo_2$ (8) are superconductors and the other compounds are temperature independent paramagnets (7). The magnetic ordering in $CeFe_2$ is thought to be associated with the iron atoms (10). Thus it is difficult to make any comments on the electronic configuration of cerium in this compound. In $CeCo_2$ and $CeRu_2$ there are probably no localized electrons because of the superconductivity. And in the $CePt_2$ and $CeAl_2$ the moment per cerium atom is 2.5 $\mu_B$ or approximately equal to that of the $Ce^{+3}$ ion with one localized 4f electron. Thus the above properties agree with the list in Table 1. The room temperature susceptibility for these compounds (7) does not agree with this list in that the value for the iridium compound is the lowest and that for the cobalt compound the highest, excluding the platinum, iron and aluminum compounds. The high value for the cobalt compound may be related to the localized unpaired electron associated with the cobalt atom rather than a localized 4f electron of the cerium atom. The band structures of these compounds may contribute to the room temperature suscepti-

bility as much as the cerium atom, especially as the number of 4f electrons per cerium decreases.

The question may be asked, why does cerium behave differently in some of these compounds than in others? To answer this it is necessary to look at the structure and properties of Laves phases.

Laves phases always have the $AB_2$ stoichiometry where the A atom is larger than the B atom. The B atoms lie on the corners of tetrahedra. In the cubic Laves phases, C15, these tetrahedra are joined point to point with the arrangement of the tetrahedra leaving holes in the lattice for the A atoms. The closest packing of hard spheres of two sizes in the above arrangement occurs if the ratio of the radius of the A atom to the B atom is 1.225. In this ideal case there are no AB contacts and the A-A contact distance and the B-B contact distance can be calculated from the lattice parameter of the compounds.

Compounds however are known to form from atoms with radius ratios far different from the ideal value. But these atoms undergo considerable mutual size readjustment to achieve the closest packing i.e. a radius ratio of 1.225. If the radius ratio $r_A/r_B$ is greater than 1.225 upon formation of the compound the A atom contracts and the B atom expands (11). It is usually found that the larger atom undergoes the larger size change and the lattice is controlled more by the more

rigid small atoms (12).

Table 2 gives some information on the radius ratios of cerium and lanthanum compounds (listed in the same order as Table 1).

Table 2. Radius ratios of cerium and lanthanum Laves phases

| Compound | $\frac{r_{Ce}^{+3}}{r_B}$ | $\frac{r_{Ce}^{+3.6}}{r_B}$ | $\frac{r_{Ce}^{cal}}{r_B}$ | Compound | $\frac{r_{La}^{+3}}{r_B}$ | $\frac{r_{La}^{cal}}{r_B}$ |
|---|---|---|---|---|---|---|
| $CeMg_2$ | 1.152 | 1.070 | 1.180 | $LaMg_2$ | 1.122 | 1.188 |
| $CeAl_2$ | 1.289 | 1.198 | 1.218 | $LaAl_2$ | 1.311 | 1.231 |
| $CePt_2$ | 1.330 | 1.236 | 1.207 | $LaPt_2$ | 1.353 | 1.209 |
| $CeRh_2$ | 1.372 | 1.275 | 1.213 | $LaRh_2$ | 1.395 | 1.230 |
| $CeIr_2$ | 1.360 | 1.264 | 1.208 | $LaIr_2$ | 1.383 | 1.226 |
| $CeOs_2$ | 1.364 | 1.268 | 1.215 | $LaOs_2$ | 1.387 | 1.237 |
| $CeNi_2$ | 1.482 | 1.376 | 1.224 | $LaNi_2$ | 1.506 | 1.261 |
| $CeRu_2$ | 1.379 | 1.281 | 1.219 | $LaRu_2$ | 1.402 | 1.244 |
| $CeCo_2$ | 1.474 | 1.370 | 1.226 | $LaCo_2$ | 1.499 | does not form |
| $CeFe_2$ | 1.449 | 1.346 | 1.240 | $LaFe_2$ | 1.473 | does not form |

$r_{Ce}^{cal}/r_B$ and $r_{La}^{cal}/r_B$ are the radius ratios determined by calculating the radius of cerium and lanthanum from the lattice parameter of the compounds and by assuming no size change for the B atom. It is obvious from Table 2 that there is a large change in rare earth atom size to adjust the $r_A/r_B$ ratio so that it approaches the ideal radius ratio value of 1.225. When the ratio gets too large as in the $LaCo_2$ case the compounds do not form. The critical ratio for the lanthanum compounds is $r_{La}^{+3}/r_B \approx 1.5$ but the nickel compound may form because a larger electronegativity difference or another effect

may counteract the size (radius ratio) effect. In the cerium case there are two alternatives to reducing the size of the cerium atom. One is by a compression of the cerium atom as happens with the lanthanum atoms. The other case would be when the cerium atom reduces its size by transferring all or part of the 4f electron into the conduction band.

It can be seen from the lanthanum data that when $r_A/r_B$ becomes greater than 1.36 the observed radius $r_{La}{}^{cal}/r_B$ becomes larger than 1.225. The same thing would be expected to be true for cerium except that for B atoms smaller than platinum the cerium atom starts transferring the 4f electron to maintain the ideal ratio of 1.225. From the observed radius ratio one would expect the transfer to be complete when the ratio starts increasing above 1.225. It would appear then that the transfer is complete for nickel as well as ruthenium, cobalt and iron compounds. Based on this analysis nickel would be expected to be a superconductor as are $CeRu_2$ and $CeCo_2$, but it is not (8).

In addition to the anomalous nickel behavior this analysis does not explain the reason why the other compounds which have a non zero $\Delta V/V_i$ (listed in Tables 1 and 2) do not fall in order of the radius ratios. There are several ways in which the above analysis is not complete. It neglects the size change of the B atoms and the effects of band structure. Whether or not the above effects are important is difficult

to tell because of the almost complete lack of data on the elastic and electronic properties of these compounds. It was with these thoughts in mind that this study of the low temperature heat capacity and magnetic susceptibility of some of these compounds were undertaken.

At the time this study was started $CeRu_2$ was the only known cerium Laves phase superconductor. For this reason it was decided to examine $CeRu_2$ as the material which had cerium atoms with the minimum amount of 4f character. $CePt_2$ was examined because platinum is about the same size as ruthenium and the cerium in the $CePt_2$ compound has one 4f electron. Furthermore, it was hoped to form pseudo-binary alloys $CePt_{2-x}Ru_x$ to study how the properties change as the valence of cerium changes. For reasons to be discussed later these alloys could not be formed. It was then decided to study the corresponding lanthanum compounds to see how the extra electron in cerium affected the properties compared to lanthanum.

Specific heat measurements at low temperatures can give information on many types of electrical and magnetic phenomenon. This information has been discussed at length in other references and only the applicable parts will be discussed here (13,14).

Most normal metallic materials have only two contributions to the specific heat, an electronic and a lattice contribution. The first contribution can be given to a good

approximation by the following:

$$C_e = (2/3)\pi^2 k^2 V\ N_{(E)} T = \gamma T \qquad (1)$$

k = Boltzmann's constant

V = molar volume

$N_{(E)}$ = number of states/volume with energies near Fermi energy

T = temperature

The important part to observe is that $C_e$ is proportional to temperature and that the proportionality constant $\gamma$ is related to the density of states near the Fermi surface. The density of states referred to here is the density of states averaged over all of the Fermi surface so that no details of the band structure are explicitly obtainable from the specific heat of the electrons. Useful information about the band structure can still be obtained particularly in the cases where measurements are made on a series of related metals and changes in $\gamma$ between alloys are used to explain changes in the band structure with alloying (15,16).

The second term, the lattice contribution for simple metals particularly at low temperatures is usually analyzed in terms of the Debye approximation which leads to the following equation:

$$C_L = \frac{12}{5} R\pi^4 \frac{T^3}{\theta_D{}^3} = \beta T^3 \qquad (2)$$

R = gas constant

Provided temperatures are low enough, the Debye characteristic temperature $\theta_D$, and thus $\beta$, are constant.

The total heat capacity can be written $C = \gamma T + \beta T^3$ where the constants $\gamma$ and $\beta$ are evaluated by plotting $C/T$ versus $T^2$.

The Debye temperature for a simple medium is related to the maximum frequency which the atoms can vibrate and as such is a simple parameter which relates thermal and elastic properties of materials. Materials with high Debye temperatures have atoms which are difficult to get in motion with thermal energy because of high interatomic forces present in the solid. Thus the Debye temperature is related to the properties of the atoms which are responsible for the rigidity of the structure.

## SAMPLE PREPARATION

The chemical analyses of the components used in this study are given in Table 3.

Table 3. Analysis of component materials

| | La | Ce | Ru | Pt |
|---|---|---|---|---|
| H | 2 | 2 | 1 | 21 |
| N | 350 | 33 | 4 | 145 |
| O | 395 | 665 | 15 | 103 |
| Mg | | <55 | FT | VFT |
| Al | | | VFT | VFT |
| Si | <15 | <30 | VFT | FT |
| Ca | <15 | <90 | FT | VFT |
| Cr | | <80 | FT | VFT |
| Fe | 105 | <20 | FT | - |
| Ni | <10 | | - | VFT |
| Cu | | <20 | Ft | VFT |
| Zr | | <200 | | |
| Ru | | | | T(X) |
| Rh | | | | T |
| Pd | | | | FT |
| Ag | | | | VFT |
| La | | <200 | | |
| Ce | <300 | | | |
| Pr | <600 | <200 | | |
| Nd | <200 | <200 | | |
| Ta | 660 | <500 | | |

- none found
< less than
T trace
FT faint trace
VFT very faint trace
(X) interference
all impurities listed as ppm by weight

On reviewing the literature on these compounds it was found that with the exception of $CeRu_2$ little was known about the phase diagrams concerning these compounds. The phase

diagram of $CeRu_2$ had been investigated and it was known that $CeRu_2$ formed peritectically from ruthenium and liquid alloy at 1570 ± 10°K (17). The phase diagram is given in Fig. 1.

Cerium and ruthenium were melted together using a conventional arc melter with a water cooled copper hearth and a gettered argon atmosphere to form the stoichiometric $CeRu_2$. A Debye-Scherrer x-ray powder pattern of a sample of the ingot showed some lines in addition to those attributable to the C15 Laves phases. A metallographic examination of the ingot revealed three phases and evidence of peritectic rimming. An attempt was made to remove the nonequilibrium microstructure by annealing the ingot at temperatures just below the eutectic temperature, 645°C. An arc melted sample heat treated 84 hours at 625°C showed no change in the amounts of the phases present. The conclusion reached was that at 625°C diffusion rates were too low for any homogenization to take place in a reasonable amount of time. At higher homogenization temperatures the low melting liquid would wet the tantalum crucibles used thereby making removal of the brittle Laves phase impossible.

It was thought that if an alloy were prepared which had a cerium concentration greater than 35 atomic per cent cerium the peritectic reaction would be avoided and no elemental ruthenium would be present in an arc melted button. The above was indeed observed. The problem then remained of how to get

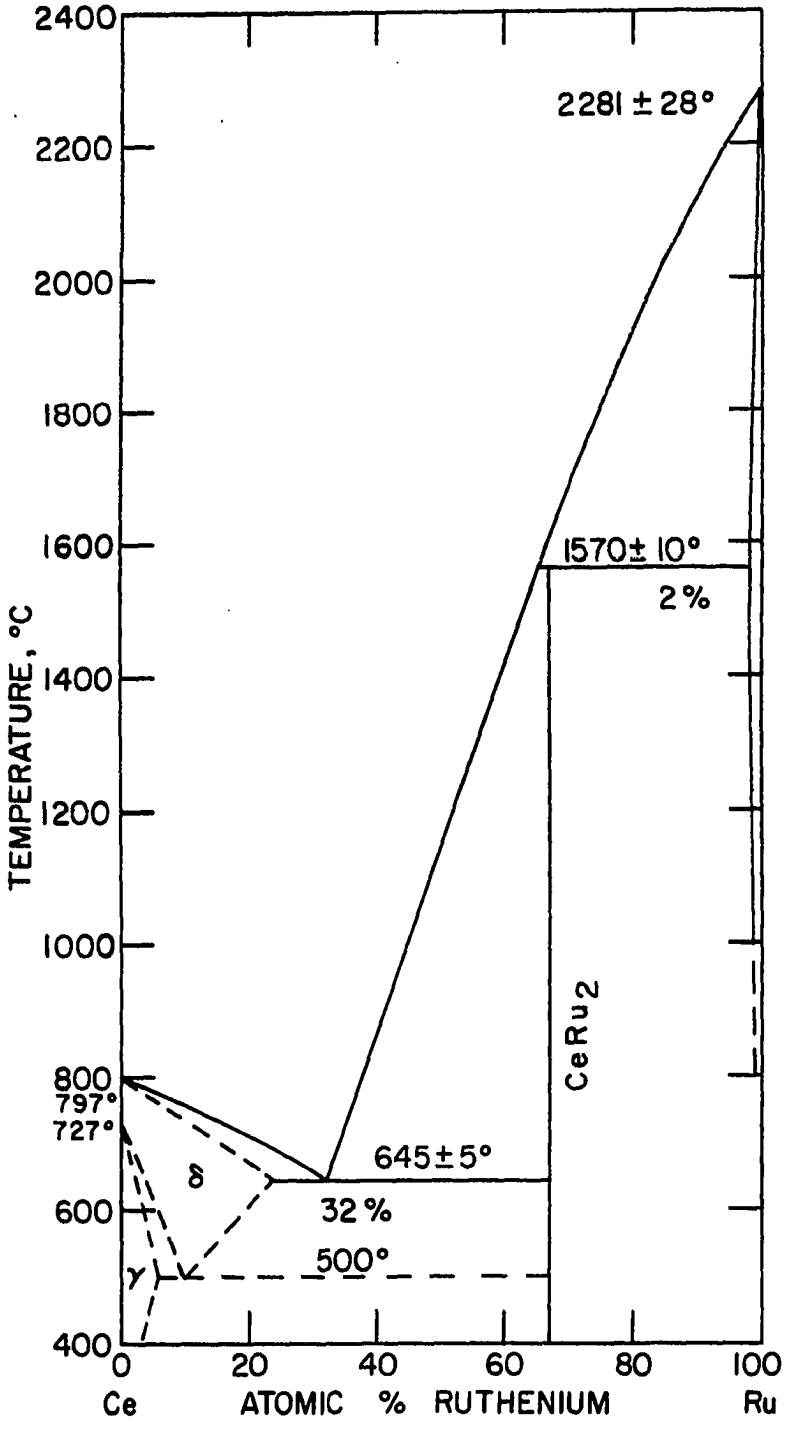


Figure 1. Cerium-ruthenium phase diagram after Obrowski (17)

rid of the cerium rich eutectic which was intermixed with the Laves phase. Leaching a powdered sample with nitric acid was found to work, but the process was messy and the resulting samples were not ideally suited for calorimetry. Another possible solution was arc zone melting (18). With this technique a sample is placed in a trough in a water cooled copper hearth and a molten zone is established at one end of the bar. If the hearth is moved under the arc the molten zone will move along the bar. Since the material freezing out of this molten zone as it moves is $CeRu_2$ the final phase distribution in the bar is in principle $CeRu_2$ in one end of the bar and the eutectic at the other end. In practice the phase separation is not complete. Metallographic point count analysis of the bars show three percent of the eutectic mixed with the $CeRu_2$. Figure 2 shows photomicrographs of some of the microstructures obtained in an arc zone melted bar. From the phase diagram it is possible to determine that the bar would contain 1.8 weight percent cerium-ruthenium solid solution if three percent of eutectic is present.

The phase diagram has not been established for the La-Ru system but on the assumption that it was similar to the Ce-Ru system an attempt was made to prepare $LaRu_2$ in a similar manner to that of $CeRu_2$. It was observed that a 35 atomic percent lanthanum sample was three phase not two phase like the cerium alloy had been.

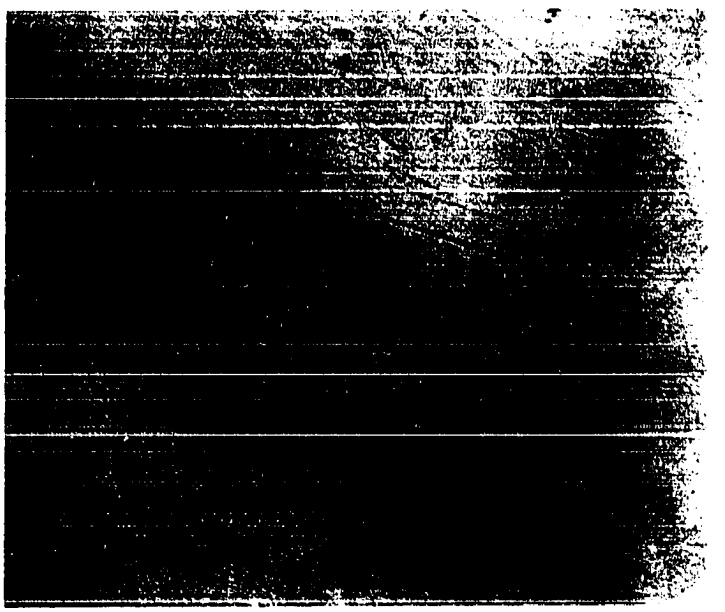

250X Nital etch

A. Absence of second phase

250X Nital etch

B. Typical second phase present

Figure 2. Photomicrographs of arc zone melted $CeRu_2$

A sample with $LaRu_2$ stoichiometry was put into a tantalum crucible which was welded closed under a helium atmosphere. This sample was homogenized at 1200°C ± 50°C for 16½ hours. There was no sign of attack of the tantalum crucible and the alloy was 99.5% single phase but with many voids present. The 0.5% of second phase present was thought to be ruthenium.

No information is available on the La-Pt or Ce-Pt phase diagrams other than that there are at least two other compounds present in these systems $RPt_5$ (19) and RPt (20). Arc melted samples of $CePt_2$ were not single phase thus indicating that these compounds also form peritectically. (Fig. 3) Homogenization of these samples was accomplished by placing the sample in a water cooled silver trough (21). The trough and sample were placed inside of a quartz tube and the tube continuously evacuated. The sample was heated by an induction method and found to be free from any crucible contamination.

Samples which were multiphase when arc melted could be made single phase by heating the sample to 1350° ± 50°C for 15 minutes and then cooling at the rate of 10 degrees per minute till a temperature of 700°C was reached. When 700°C was reached the power could be shut off and the sample cooled rapidly to room temperature. Figure 3 shows how clean a sample could be prepared with this technique i.e. there was no second phase present.

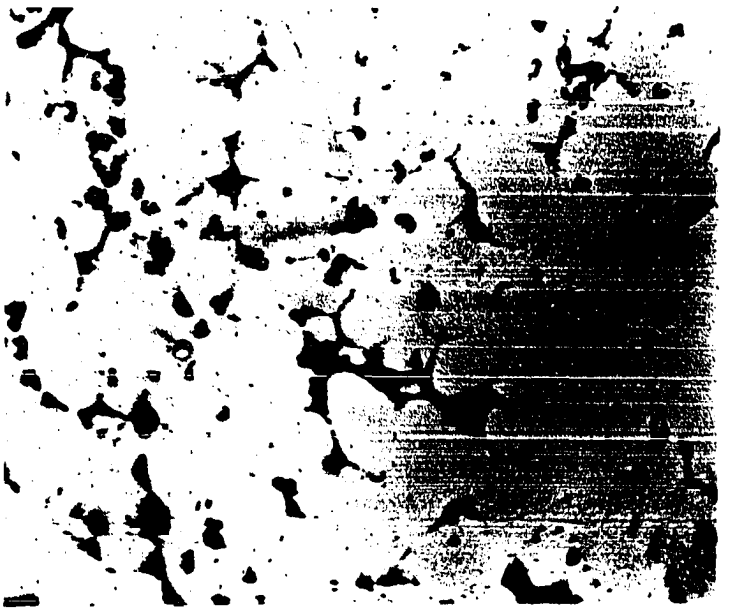

250X Etch $3HNO_3$-2HCl

A. Arc melted sample

250X Etch $3NHO_3$-2HCl

B. Homogenized sample

Figure 3. Photomicrographs of $CePt_2$

The $CePt_2$ and $LaPt_2$ samples were reactive in air. The samples would crumble into powder if left unprotected. A metallographic sample left in the polished condition would show many cracks after a few days. These cracks did not follow any second phase and they were transgranular. The samples were protected by sealing them in helium filled vials. When sealed in the above manner the sample had no tendency to crumble and a polished surface remained bright.

As usual for ternary systems, there is no data in the literature on the pseudo-binary system $CePt_{2-x}Ru_x$. In an attempt to determine if a continuous solid solution exists between $CePt_2$ and $CeRu_2$ small buttons (6 gm) were prepared of compositions corresponding to intermediate alloys. These buttons were examined metallographically and they were all found to be multiphase. Debye-Scherrer powder patterns and standard extrapolation techniques were used to determine the lattice parameters of the Laves phase present in the buttons. The lattice parameter data (Fig. 4) do not follow a smooth curve between the two end components as would be expected if complete solid solubility existed. Also, extra lines start appearing on the x-ray patterns as one moves away from the end components. It was suspected from the above information that a new phase existed somewhere between the end components. X-ray microprobe analysis of the CePtRu alloy which had been annealed at 1375°C for 312 hours showed the existence of two

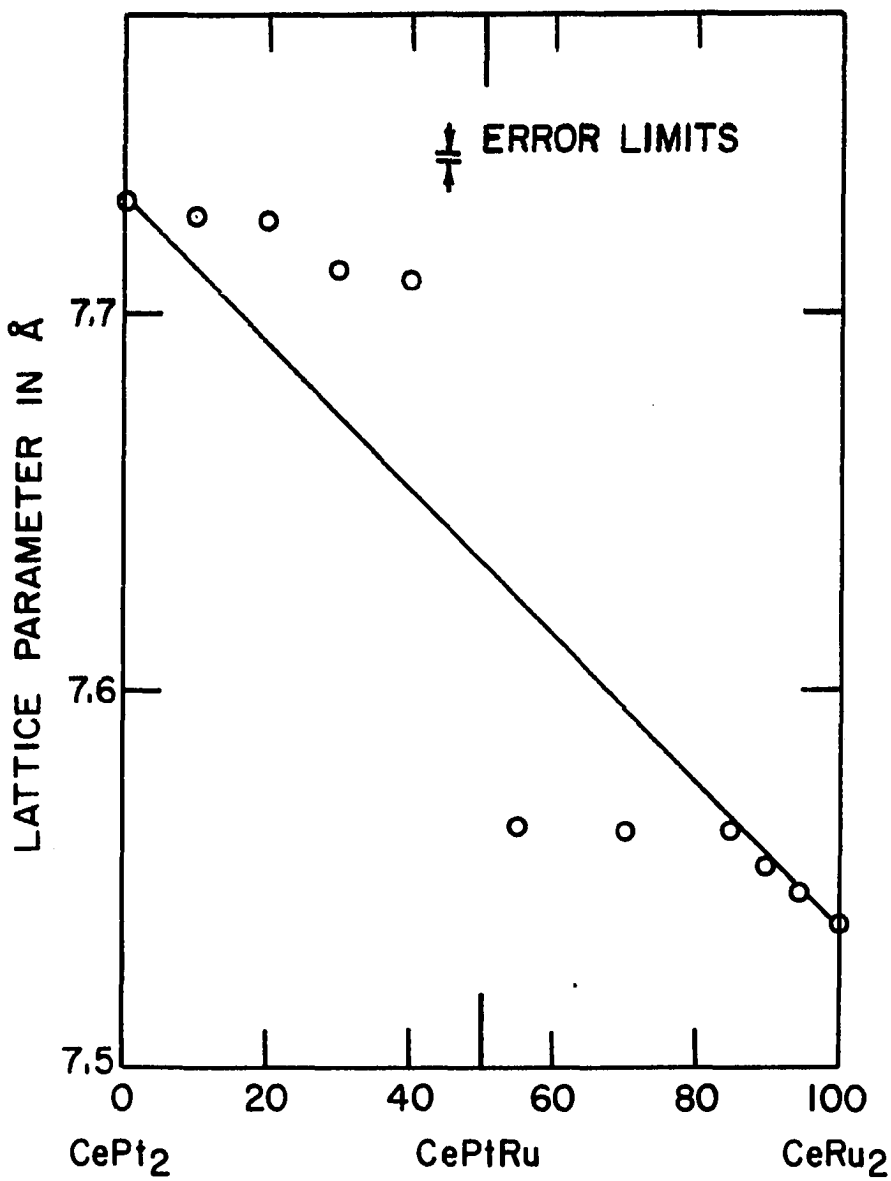


Figure 4. Lattice parameters in system $CePt_{2-x}Ru_x$

phases. One phase was equi-atomic CePt and the other pure ruthenium. The microprobe analysis was confirmed by comparing the lines of the powder pattern with the lines expected for pure ruthenium and the compound CePt, which has the $B_f$ (20) (B33, TlI) (22) structure. The measured 2θ values are compared with the generated values in Table 4.

Table 4. Comparison of x-ray data on CePtRu

| Observed CePtRu | | Generated[a] CePt | | | Ruthenium | |
|---|---|---|---|---|---|---|
| Intensity | 2θ | $I_{cal}$ | hkℓ | 2θ | hkℓ | 2θ |
| VVW | 23.97 | 181 | 110 | 24.12 | | |
| VVW | 28.42 | | | | | |
| VS | 31.42 | 899 | 111 | 31.28 | | |
| W | 32.82 | 370 | 130 | 33.50 | | |
| VW | 34.82 | | | | | |
| VW | 36.97 | | | | | |
| M | 38.47 | 401 | 041 | 38.51 | | |
| VS | 39.27 | 1000 | 131 | 39.20 | 100 | 38.2 |
| M | 42.32 | | | | 002 | 42.2 |
| VS | 44.12 | | | | 101 | 44.0 |
| VVW | 46.22 | 250 | 200 | 46.3 | | |
| M | 58.47 | | | | 102 | 58.2 |
| W | 69.57 | | | | 110 | 69.2 |
| M | 78.47 | | | | 103 | 78.4 |
| W | 81.02 | | | | 200 | 82.2 |
| M | 84.82 | | | | 112 | 84.6 |
| W | 86.07 | | | | 201 | 86.1 |
| VW | 116.72 | | | | 203 | 116.6 |
| VW | 121.02 | | | | 210 | 121 |
| VS | 125.17 | | | | 211 | 125.2 |
| S | 133.12 | | | | 114 | 133.6 |
| VW | 140.37 | | | | 212 | 141.0 |
| M | 146.47 | | | | 105 | 146.6 |

[a]Values used were: x = 0.135 for Ce; y = 0.135 for Pt; a = 3.921; b = 10.920; c = 4.524. (20)

The CePtRu sample used here was prepared by arc melting together appropriate amounts of the compounds $CePt_2$ and $CeRu_2$. This indicates that CePt is so stable compared to $CeRu_2$ that it removes the cerium atoms from the ruthenium atoms.

It would appear from Fig. 4 that alloys with greater ruthenium content than $CePt_{0.3}Ru_{1.7}$ might not be multi-phase. But several attempts to prepare single phase samples in this region all met with failure. Microprobe analysis of a $CePt_{0.1}Ru_{1.9}$ alloy after arc zone melting showed the presence of the phase CePt. Furthermore, it was not possible to produce single phase platinum rich alloys.

# CALORIMETRY

## Apparatus

The low temperature calorimeter construction during this project was designed so that measurements could be made in a magnet with a pole gap of 5 cm. This restriction meant that the diameter of the helium space was 2.8 cm. (Fig. 5) To keep within this diameter the construction of the calorimeter had to be very sophisticated or very simple. We chose the simple approach at the expense of the loss of some accuracy because we felt the results we desired would not need to be known to more than a few per cent. The calorimeter is the heat pulse type where a sample is thermally isolated from the surroundings. A pulse of electrical heat is applied to the sample for a known length of time, and from the temperature rise of the sample during that time interval and the heat input the specific heat of the sample can be determined.

The dewar for the calorimeter (Fig. 5) is of conventional double wall design with a liquid nitrogen shield surrounding the helium space. To conserve space the lower part of the shield is not a layer of liquid nitrogen but a copper shield in contact with the nitrogen bath. Provisions are made to connect the helium space to a 115 CFM vacuum pump to lower the pressure above the helium bath. The calorimeter is suspended from the top of the dewar by three stainless steel tubes. One of the tubes leads to the vapor pressure bulb. One is

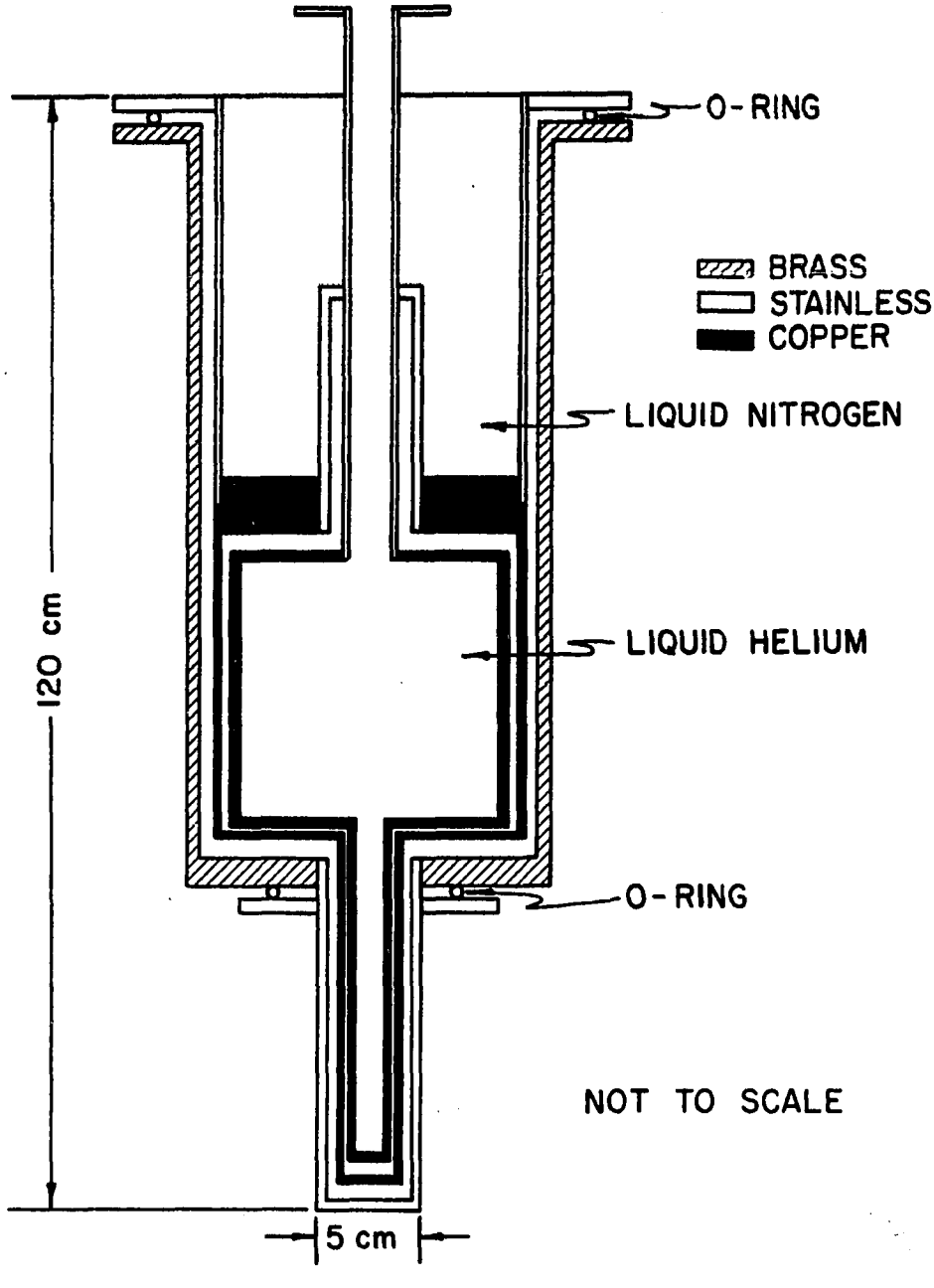


Figure 5. Drawing of dewar assembly

the vacuum line to the calorimeter and contains the wire used to raise and lower the sample in order to make or break thermal contact with the bath. The other tube contains the electrical leads. The third tube is sealed at both ends with epoxy and filled with a low viscosity silicon oil to thermally short the leads to the bath.

To further insure that the electrical leads are at bath temperature about 45 cm of the electrical leads are wrapped around the post which is at bath temperature (Fig. 6). The leads are then cemented to the post with General Electric 7031 varnish. About 15 cm of the leads are left free in the calorimeter before connecting onto the addenda to provide a long heat leak path. The vapor pressure bulb is located in the post. The tube which leads from the vapor pressure bulb to the manometers is vacuum jacketed to above the helium liquid level to prevent any cold spots from developing along the tube.

The addenda is suspended from a 12 cm piece of nylon fish line which is connected to a 0.25 mm stainless steel wire which goes to the top of the calorimeter where it connects to a shaft. The shaft which is sealed into the calorimeter vacuum space with an O-ring can be moved vertically to bring the addenda in contact with the bath. The stainless steel wire is thermally grounded to the bath by means of a copper wire. The top surface of the addenda is indium coated as well as the mating surface of the post.

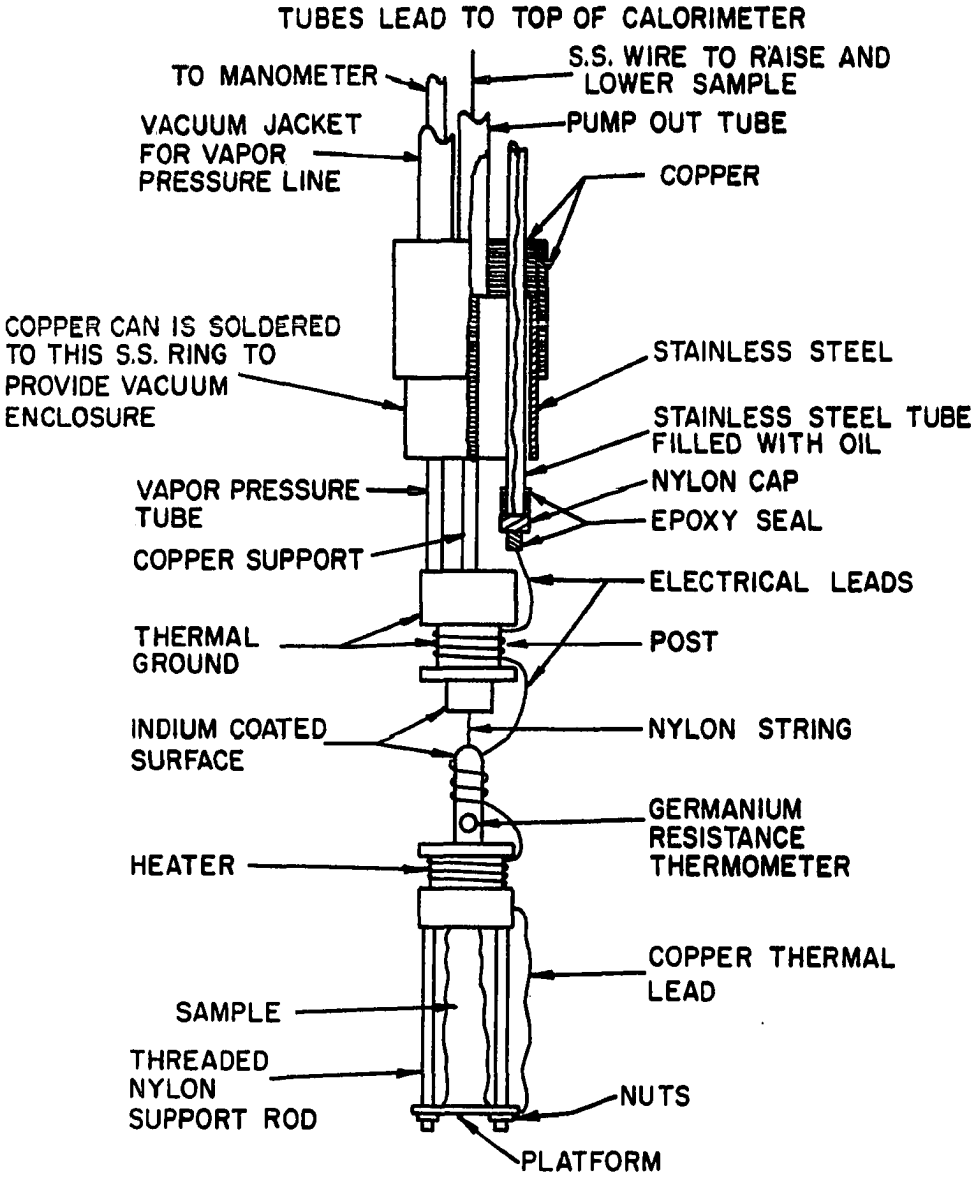


Figure 6. Calorimeter assembly

The addenda consists of a sample holder which has the germanium resistance thermometer and sample heater mounted on it. The sample holder maintains the sample (in the shape of a rod or cube) in contact at all temperatures by means of a platform suspended on three threaded nylon screws. Nylon screws are used so that the contraction during cooling keeps the sample in contact with the copper piece on which the germanium resistance thermometer and heater are mounted. The maximum size sample which can be measured depends on whether or not the sample can be drilled to accomodate the nylon screws. The maximum size sample that has been measured was the 8 $cm^3$ copper standard.

Sample cooling from 77°K to 4.2°K was achieved by bringing the mating surfaces of the addenda and post together. About an hour was necessary to cool the sample to 4.2°K. The thermal switch was opened by lowering the wire causing the sample and addenda to break the contact. The isolation of the sample causes some heating to occur at the lowest temperatures but since the calibration of the thermometer does not extend to the lowest temperatures this is not a problem. With the bath at 1.2°K and the sample at 4.2°K the amount of the heat leak from the sample to the bath is 1 $\mu$ watt.

## Temperature Measurement

The temperature of the sample was measured by means of a Honeywell Type II germanium resistance thermometer (GRT).

The establishment of the resistance versus temperature curve will be discussed in the section on thermometry. The GRT is a four lead resister and the leads used in the calorimeter were #40 cotton insulated manganin wire. Current to the resistor was maintained at either 1 μ amp. or 10 μ amp. depending upon the temperature. The current for the GRT was provided by 10 mercury cells in series (Fig. 7) and was monitored by having the current go through a 1000 ± 0.01 Ω standard resistor and checking the voltage drop. The voltage drop across the resistor was checked at 10 minute intervals with the auxiliary emf terminals of a Leeds and Northrup K-3 potentiometer. The drift of the GRT current was considered to be negligible.

The voltage drop across the GRT was measured using a Leeds and Northrup K-3 potentiometer and a high input impedance Keithley 153 microvolt-ammeter as a null detector-amplifier. The drift in temperature of the sample was measured by bucking-out most of the emf ($E_1$ and $E_2$) from the GRT with the potentiometer and using the microvolt-ammeter to measure the difference between the potentiometer reading and null ($E_1'$ and $E_2'$). The difference was amplified by the microvolt-ammeter and displayed on a chart recorder (Texas Inst. Servo-riter II). The green pen (0-10 mv) of the strip chart recorder was used at a chart speed of 6"/min (15 cm/min).

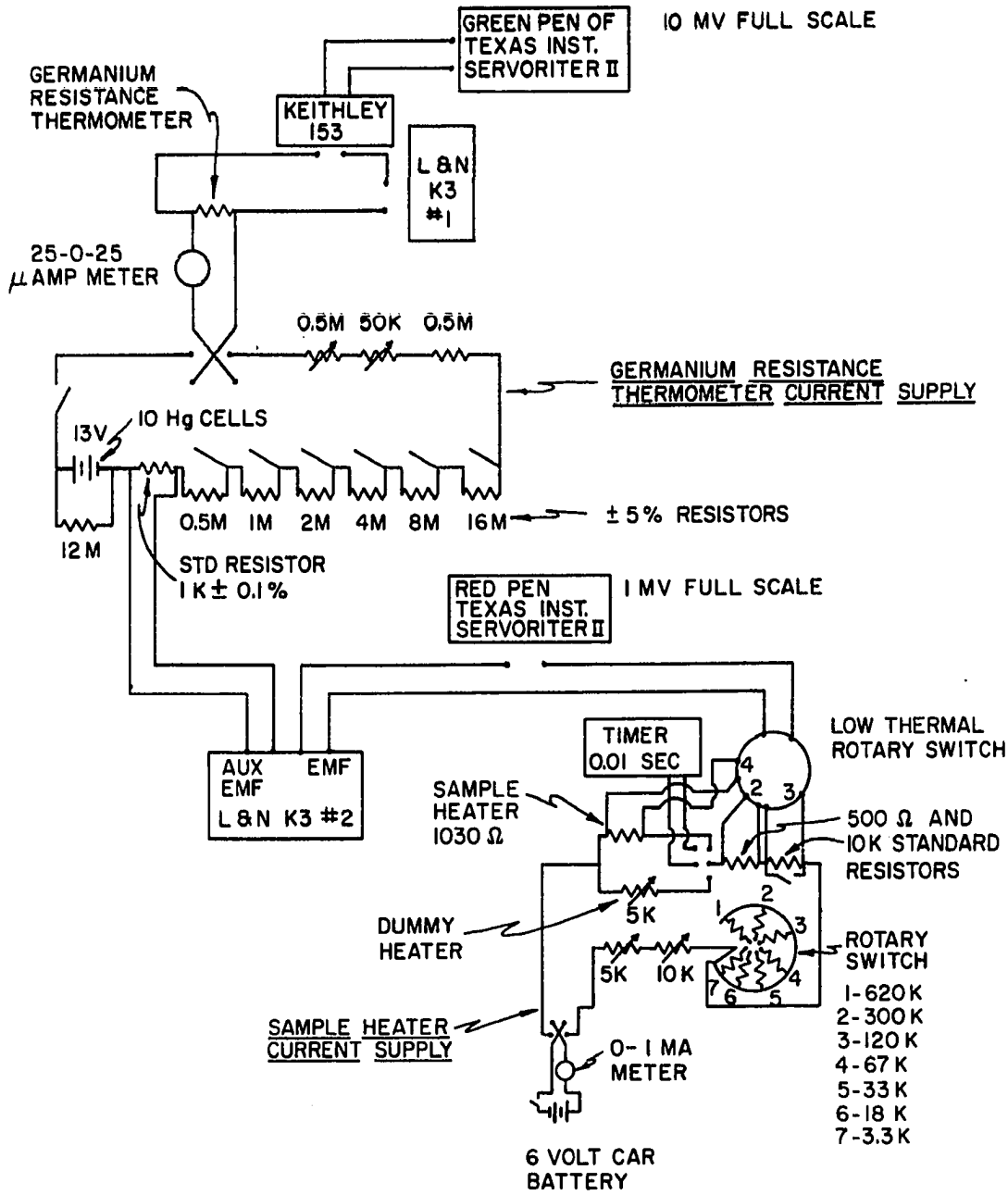


Figure 7. Calorimeter electrical circuitry

## Heater Current Measurement

The sample heater (Fig. 7) which is part of the addenda is 1030 Ω of noninductively wound manganin wire cemented to the addenda with General Electric 7031 varnish. The current leads are #30 manganin wire while the potential leads are #40 manganin. The current source is a 6 volt car battery in series with a variable resistance. Currents from 30 μ amp to 1000 μ amp are obtained with the above arrangement.

The current normally flows through a dummy heater which has the same resistance as the sample heater. This is to keep the battery conditioned so that a sudden change in current does not occur. When the current is switched from the dummy to the sample heater the clutch on the timer (Standard Electric Time Co. SW-1) is engaged so that the elapsed time that the current is running through the sample heater may be determined. The timer reads to 0.01 sec without interpolation.

The current through the heater is determined by passing the current through two standard resistors 500 Ω and 10,000 Ω. The major portion of the voltage drop from one of these resistors is balanced by a Leeds and Northup K-3 potentiometer. The remaining voltage is displayed on the chart recorder using the 0-1 mv pen. If the current to the heater is greater than 150 μ amp the 500 Ω resistor is used, otherwise the 10,000 Ω resistor is used. By this technique the

current can be read to 0.1 percent under the worst conditions, typically, however, the current is known to 0.01 percent.

To determine the resistance of the heater as a function of temperature the voltage drop across the heater with known currents and at known temperatures was measured. The resistance varied from 1029 $\Omega$ at 1.4°K to 1035 $\Omega$ at 9°K and it was reproducible to 0.1 percent upon thermal cycling between room temperature and 4.2°K. The resistance to the nearest ohm for each heat capacity point was determined from a plot of heater resistance versus resistance of the GRT. The resistance of the heater leads between the post and the addenda was determined to be 11.6 $\Omega$ . A correction for the amount of heat generated in these leads being taken as (23)

$$\Delta Q = I_H^2 R/2 \qquad (3)$$

$I_H$ = current through leads and heater

R = resistance of leads (11.6$\Omega$ ).

## Data Acquisition and Reduction

To determine the heat capacity of a sample the sample, which is usually a 20 gm rod with an eliptical cross section, is ground so that the ends are roughly parallel. The ends are then ground and polished similar to a metallographic sample. The ends of the sample are then smeared with 0.1 cc of Apiezon N grease to improve thermal contact and the

sample is mounted on the platform of the addenda. The nuts on the nylon screws are tightened down till they are hand tight. If tightened too much, the strain in the contracting nylon screws as the temperature is lowered will break the screws.

The copper can is then slipped up around the sample and the addenda and soft soldered to the stainless steel ring. The joint is the tongue and groove type. Care is taken that the GRT is not heated in the soldering process. If the GRT were heated above 100°C its calibration would change. The calorimeter is then leak checked and placed in the dewar. The sample is kept overnight with liquid nitrogen in the dewar. Only mechanical contact is used to cool the sample. Liquid helium is transferred and the sample cooled to 4.2°K. If data are to be taken above 4.2°K the sample is isolated and the run begun. If not the bath is pumped on till the temperature drops below 1.4°K.

The output voltage from the microvolt-ammeter to the recorder is adjusted so that full scale on the microvolt-ammeter corresponds to full scale on the recorder. The sample is then isolated by lowering the stainless steel wire. The two K-3 potentiometers are adjusted so that the emf readings are on the chart (Fig. 8). The temperature drift of the sample is recorded on the chart for about a minute then the current is switched from the dummy heater to the sample

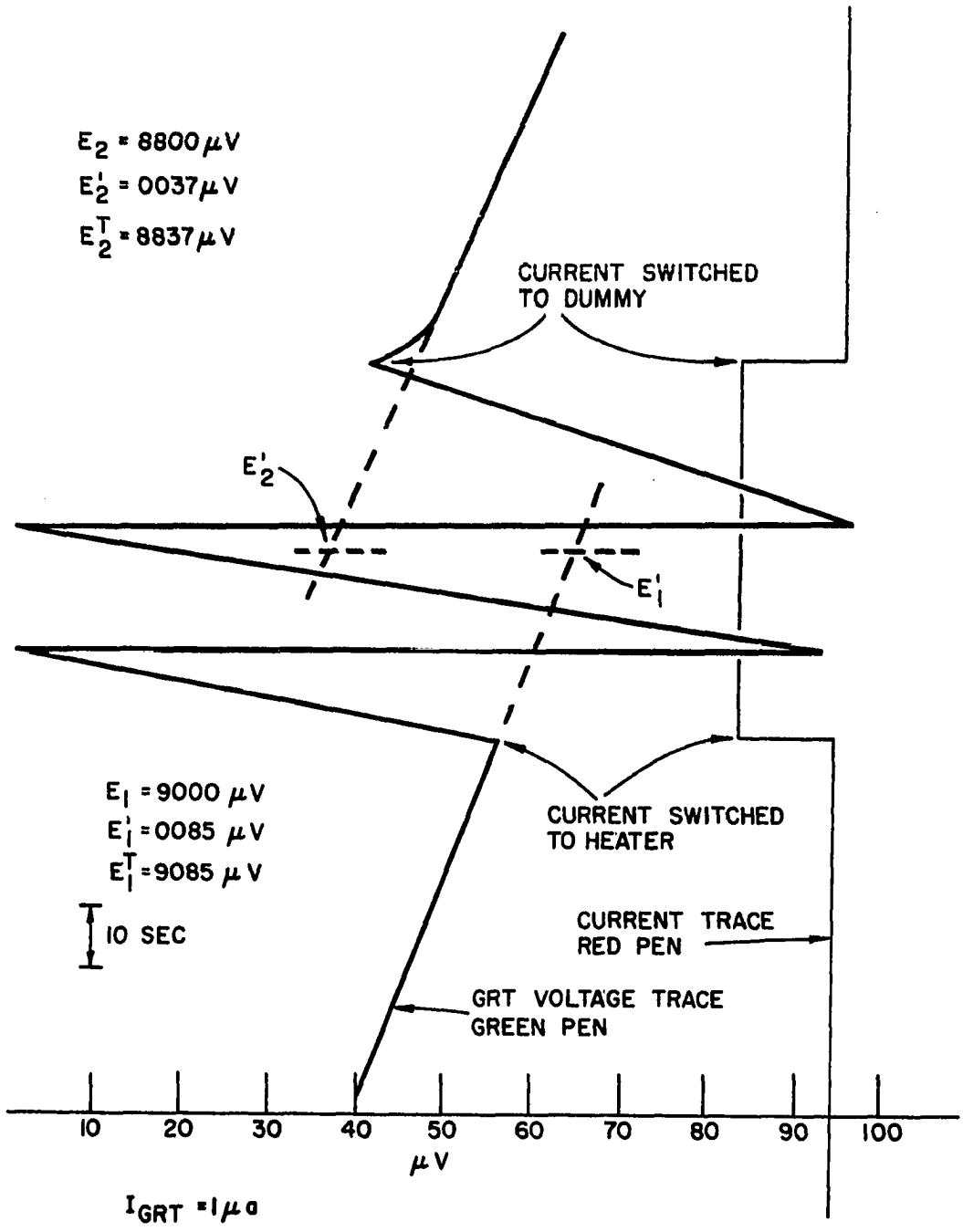


Figure 8. Schematic of typical heat capacity point

heater simultaneously turning on the timer. The setting on the potentiometer is adjusted to keep the pen on the chart. After the necessary time interval was reached the current was switched back to the dummy heater turning off the timer. The drift rate was again recorded for one minute after the rate became linear, usually in about 10 seconds.

The current through the heater was previously adjusted to give $\Delta T = T/30$ (T = temp.) for heating periods which ran from 20 sec to 120 sec. No systematic deviation was ever detected which could be related to either the heating current used or the length of the heating period although several attempts were made to observe same. The GRT potentiometer setting before and after the heat pulse was recorded as well as the elapsed time and the heater current potentiometer setting. The timer is reset to zero and the calorimeter is ready to take another data point.

To compensate for the heat leaking from the sample during the heat pulse the drift rates before and after the heat pulse are extrapolated to the midpoint of the heat pulse to determine the off null voltages $E_1'$ and $E_2'$ (Fig. 8). The $E_1'$ and $E_2'$ values are added to $E_1$ and $E_2$ to give $E_1^T$ and $E_2^T$. $E_1^T$ and $E_2^T$ divided by the GRT current, $I_{GRT}$, give the resistances of the GRT which are then converted to temperatures, $T_1$ and $T_2$, by an established equation (see section on thermometry). The current through the heater is determined by adding

the voltage from the red pen on the chart to the potentiometer reading and dividing by the standard resistor being used (500 $\Omega$ or 10,000$\Omega$). A computer is used to calculate the specific heat using the following equation

$$CN = \frac{(I_H^2 R_H + \Delta Q)\Delta t}{T_2 - T_1} - C_{Add}(T) \qquad (4)$$

C = specific heat

N = number of moles

$C_{Add}(T)$ = heat capacity of addenda

$R_H$ = heater resistance

$\Delta t$ = elapsed time of heat pulse

$I_H$ = heater current

$\Delta Q$ = correction due heater leads (see Eq. 3)

$T_2$ = temperature after pulse

$T_1$ = temperature before pulse

The output of the computer program is C, C/T, T, $T^2$ and percent of the total heat capacity represented by the addenda. A computer plot of C/T versus $T^2$ is generated as well as cards with C/T versus $T^2$ for later least squares fitting.

The heat capacity of the addenda was measured in a series of experiments to determine the quantity $C_{Add}(T)$ needed in Equation 4. The 70 heat capacity points were least squares fit to an equation of the form

$$C_{Add}(T) = AT + BT^3 + CT^5 \qquad (5)$$

The data points fit the equation with an average fractional deviation 1.6%. The scatter being associated with the high drift rate present for these early runs.

## Thermometry

Thermometry is one of the most important parts of low temperature calorimetry because of the necessity to know very small increments of temperature very accurately. Germanium resistance thermometers are ideal for heat capacity measurements in the range of temperatures of interest here 1.4-9°K. They have a small heat capacity, are independent of thermal history and have the necessary temperature sensitivity (24).

The GRT (#598) used during this investigation was calibrated over two temperature ranges. It was first calibrated over the range 4.2-22°K by comparing its resistance with another GRT (#3) which had been previously calibrated using gas bulb thermometry (25)[a]. In the temperature range 4-9°K 66 comparison points were taken which were fit to an equation of the form

$$\mathrm{Ln}T = \sum_{n=0}^{7} A_n (\mathrm{Ln}\,\frac{R}{R_o})^n \,. \qquad (6)$$

The seventh degree fit gave a root mean square deviation of T(cal) from T(obs) which was $2.15 \times 10^{-3}$ deg.

---

[a]This calibration differs from a more recent one (26) by +10 mdeg at 6°K to -10 mdeg at 4°K.

In the temperature range 1.4 to 4.2°K the GRT (#598) was calibrated against the vapor pressure of $He^4$. A vapor pressure bulb with the resistor placed in contact with the bulb was used to establish the calibration. The gas line to the manometers was vacuum jacketed to prevent any place along the line from being colder than the bulb. Two manometers constructed of 9.2 mm precision bore tubing were used to measure the vapor pressure. One of the manometers was filled with mercury and the other with butyl phthalate oil. Pressures were read to 0.1 mm with a Gaertner Scientific Corporation cathetometer. Between 1.2 and 4.2°K 68 points of pressure versus resistance were taken. The pressures were converted to temperatures, after corrections were made for room temperature and acceleration of gravity, using the 1958 helium vapor pressure scale (27). The temperatures and resistances were fit to Equation 6 using a least squares method. The fit gave a root mean square deviation of T(cal) from T(obs) of $2.2 \times 10^{-3}$ deg. The slope of the fit dR/dT was very smooth almost linear between 1.4°K and 4.0°K.

To check out the operation of the calorimeter and the validity of the thermometry a Calorimetry Conference Copper Standard was obtained (28). The specific heat of a 1.1 mole piece of the copper standard was measured from 1.4°K to 8°K and the results compared with the reference equation given for this copper standard (28) (Fig. 9). All but two of the

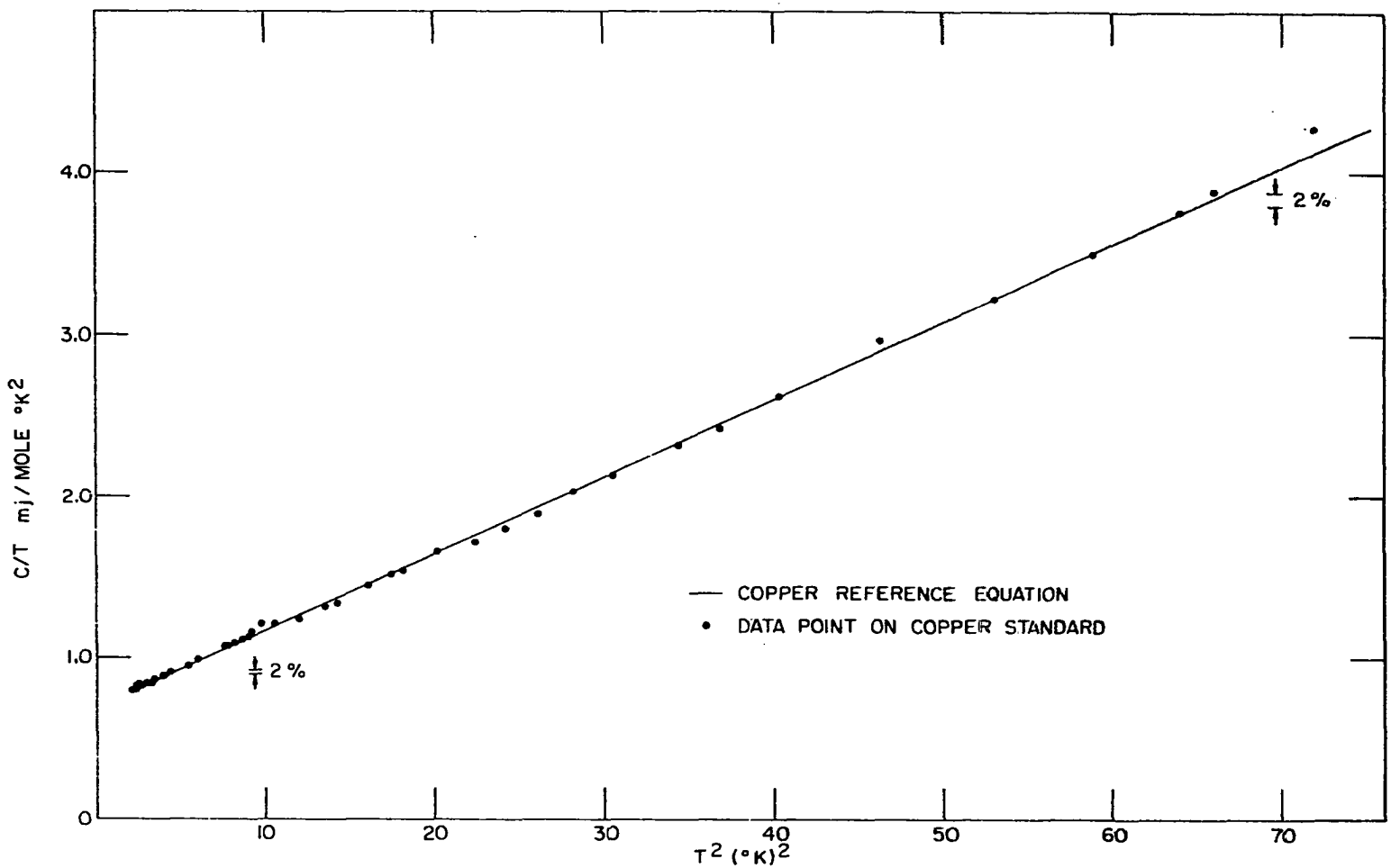


Figure 9. Specific heat of Calorimetry Conference Copper Standard

points fall within two percent of the reference equation with no systematic deviations thereby giving confidence to the two thermometer calibrations.

Measurements of heat capacity in a magnetic field were made using an electromagnet with 10 cm diameter pole tips and a 5 cm pole gap. The current for the magnet came from a motor-generator. It was found that the change of resistance of the GRT above 4.2°K was negligible in fields of 9000 oe ($<5\Omega$). Below 4.2°K the change in resistance varied from 1.3 percent of R at 3.3°K to 2.3 percent at 1.6°K. The change in R at 9000 oe was fit to an equation of the form

$$R_0 - R_{9000} = (R_{9000})^A + e^B \qquad A = 1.205 \qquad B = 0.0461 \tag{7}$$

This equation was incorporated into the computer program to correct for the effect of the field. The maximum effect of this correction was a one percent change in heat capacity. Specific heat measurements were usually made by cooling the sample in zero field, then applying the field and taking the data in constant field.

## Errors

All specific heat data in zero field were taken in at least two separate runs with the sample warmed to room temperature between runs. No systematic deviation of the specific heat from one run to the next was found. Since $I_H$ and $\Delta t$ are

known to 0.1 percent or better it is felt that most of the errors associated with the measurement of the specific heat are random in nature and associated with determining $\Delta T$ by making the extrapolations on the chart paper. The scatter in the data varied from 5 percent for the addenda and $LaPt_2$ to 2 percent for the copper standard. Some systematic error was introduced because the heat capacity of the addenda was not negligible. The addenda heat capacity amounted to about 20 percent of the total heat capacity of most samples but for the low specific heat sample $LaPt_2$ it was about 60 percent. Systematic errors may exist from the thermometry but their magnitudes are difficult to assess particularly in light of the fluctuation of the accepted temperature scale (26).

## Magnetic Susceptibility Measurement

Measurement of magnetic susceptibility were made using a vibrating sample magnetometer (29). A small irregular shaped sample is placed on the end of rod, which is made to vibrate causing the magnetic moment of the sample to induce a voltage in a set of pick up coils located around the sample. A reference voltage is established using as a standard the saturation moment of nickel at room temperature. The voltage from the pick up coils is then compared with the reference voltage to determine the moment of the sample. The sample rod is placed in a liquid helium dewar of conventional design. The sample temperature is measured with Au-Fe and Au-Co versus

copper thermocouples (30). Measurements are possible in temperature range 1.3 to 300°K.

It was discovered during the course of this work that the contribution to the susceptibility due to the sample holder was not negligible for samples with small susceptibilities (less than $3 \times 10^{-6}$ emu/cc). Thus susceptibility measurements were restricted to samples which have a localized electron, i.e. the $CePt_2$ sample.

# RESULTS AND DISCUSSION

## $CePt_2$ and $LaPt_2$

A review of the literature on the electrical and magnetic properties of the compound $CePt_2$ produced only one reference. In this work the magnetic susceptibility was measured from 77°K to 473°K. It was found that the susceptibility obeyed a Curie-Weiss law with a $\Lambda$ value of -40°K and an effective moment of 2.33 $\mu_B$.

Measurements of the magnetic susceptibility of a 0.3 gm sample of $CePt_2$ were made over the temperature range 1.3 to 70°K. The data are plotted in Fig. 10 as 1/X versus temperature. It can be seen that the sample starts deviating from Curie-Weiss behavior at about 3°K. Plots of magnetization versus field also show deviations from linearity at temperatures between 2.7°K and 3.85°K, Fig. 11. The data in Fig. 10 with the exception of the two lowest points were fitted to a straight line by a least squares method. The value of the intercept with the temperature axis is $\Delta = 0.5 \pm .7$°K and the effective moment calculated from the slope is $2.47 \pm .03$ $\mu_B$ compared to 2.54 $\mu_B$ for the theoretical $Ce^{+3}$ ion. Close agreement between theory and experiment for the compounds $RPt_2$ (where R is Pr, Nd, Gd, Ty, Ho and Er) was also found for measurements in the paramagnetic region (31). Measurements in the ordered region (31,32) of the above compounds indicate a moment less than theoretical. Because the moment

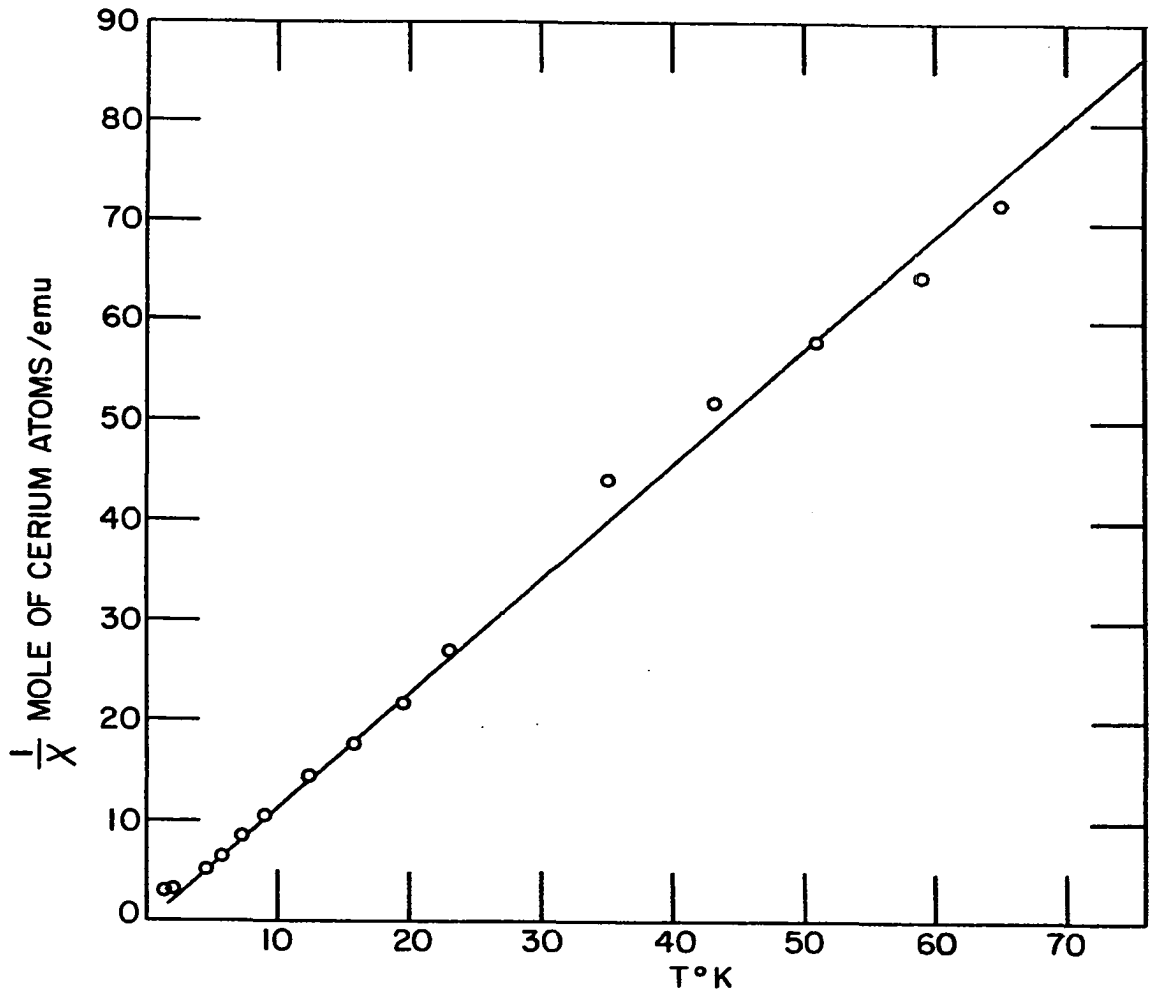


Figure 10. Inverse magnetic susceptibility of $CePt_2$ versus temperature

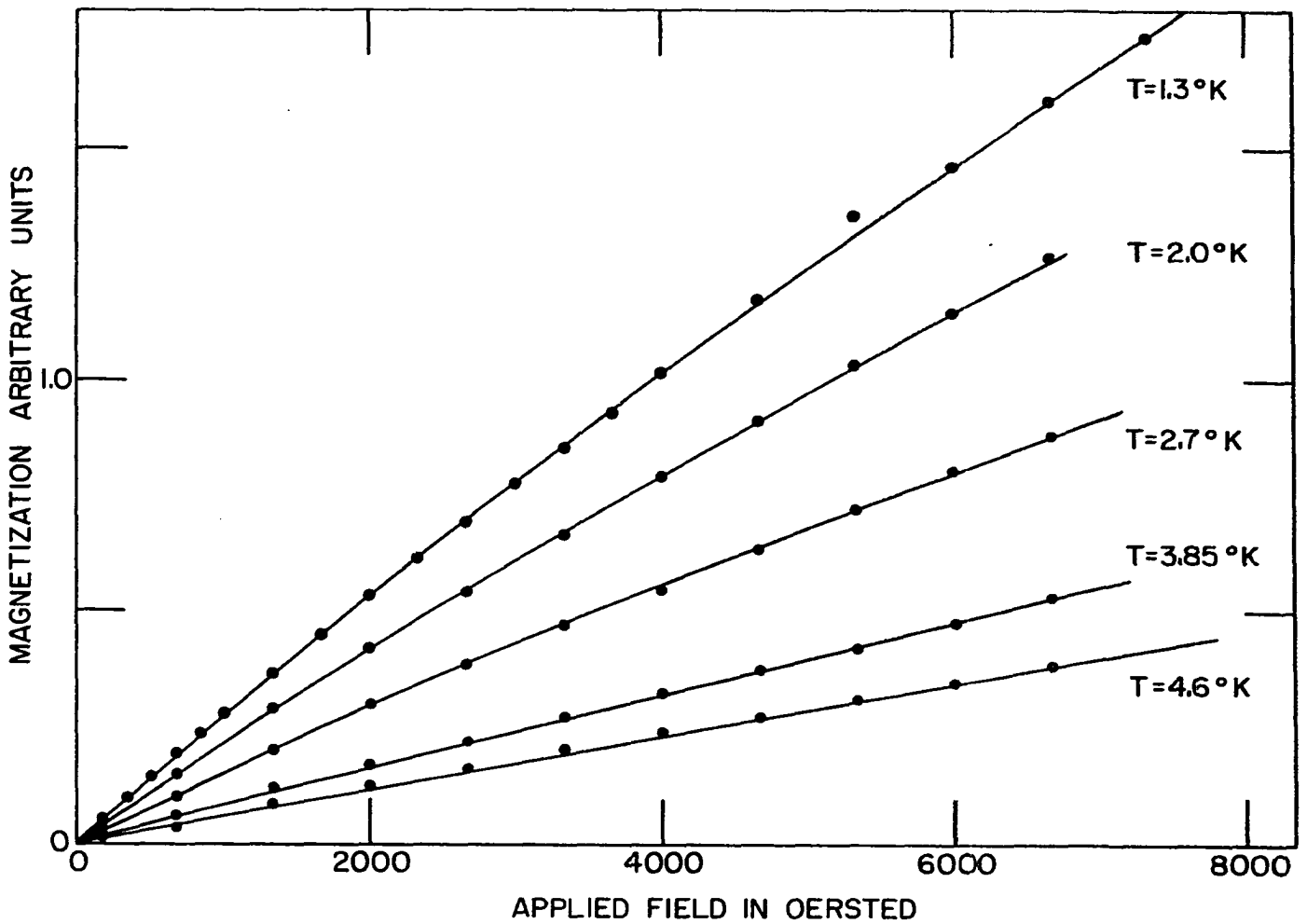


Figure 11. Magnetization versus field for $CePt_2$

in the paramagnetic region is close to theoretical the reduced moment in the ordered region is not due to crystal field effects (31). Also the deviation from Curie-Weiss behavior must not be due to crystal field splittings. Since $J = 5/2$ for cerium the ground state would be a Kramers doublet in a crystal field which would cause the susceptibility to increase faster than that predicted by Curie-Weiss behavior, not decrease as is observed. The above behavior can be explained if magnetic ordering occurs and this possibility will be discussed when the specific heat data are considered.

The specific heat of an 11 gm sample of $CePt_2$ was determined from 1.4 to 9°K. The data in Fig. 12 plotted as C/T versus T show a large peak at 1.7°K. To determine if the peak was due to crystal field splittings of the energy levels (Schottky anomaly) a calculation was done of the specific heat that would be expected (14). The specific heat was calculated using a two level model with equal degeneracies of the levels. The Schottky specific heat is shown in Fig. 13 superimposed on the measured specific heat. As can be seen the agreement is not very good and it is not expected that other possible level schemes would give better agreement. That is, the Schottky type anomalies would give broad type peaks compared to the sharp peak observed. Thus the specific heat data is in agreement with the susceptibility data that at low temperatures crystal field effects are not the dominant effect.

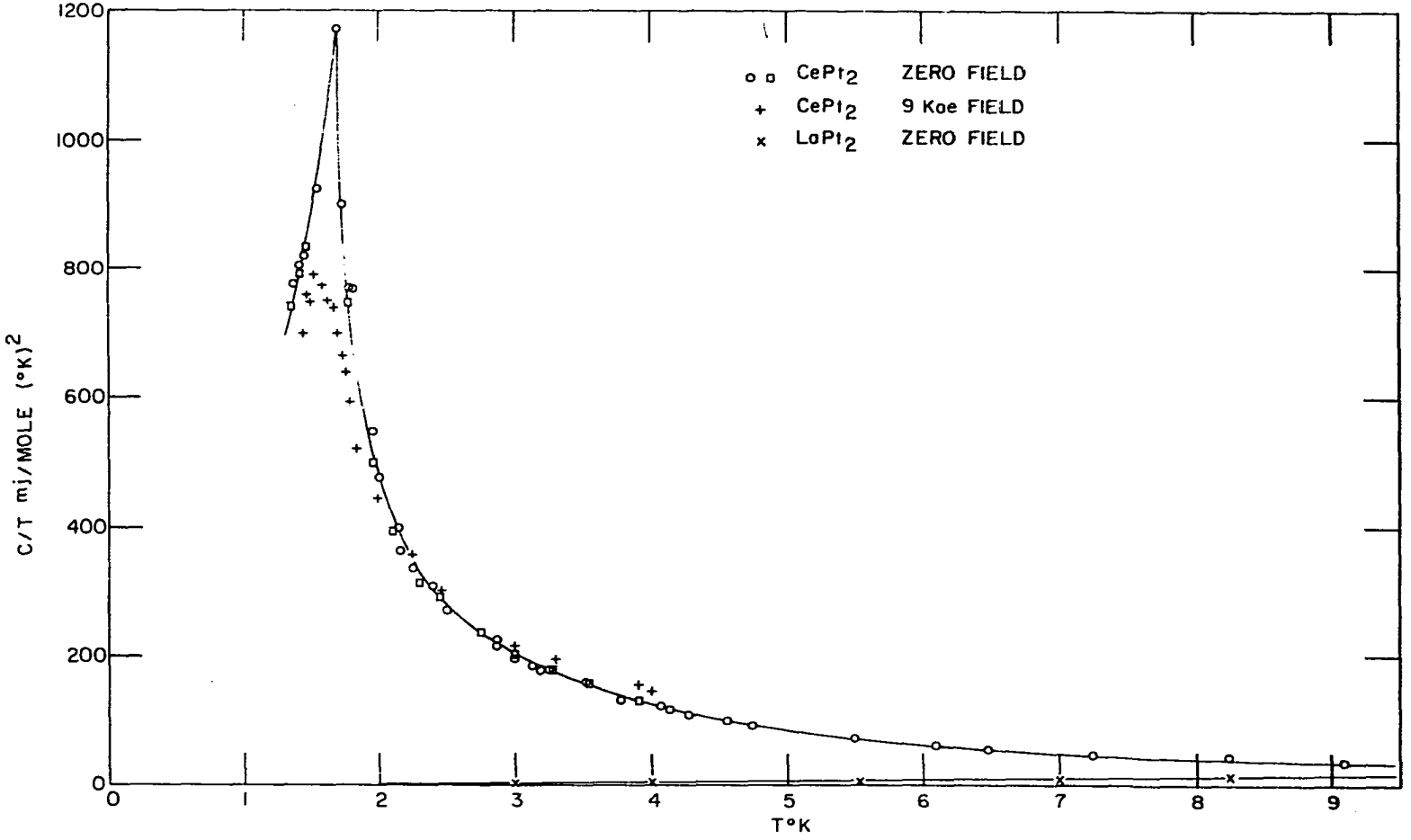


Figure 12. Specific heat of $CePt_2$

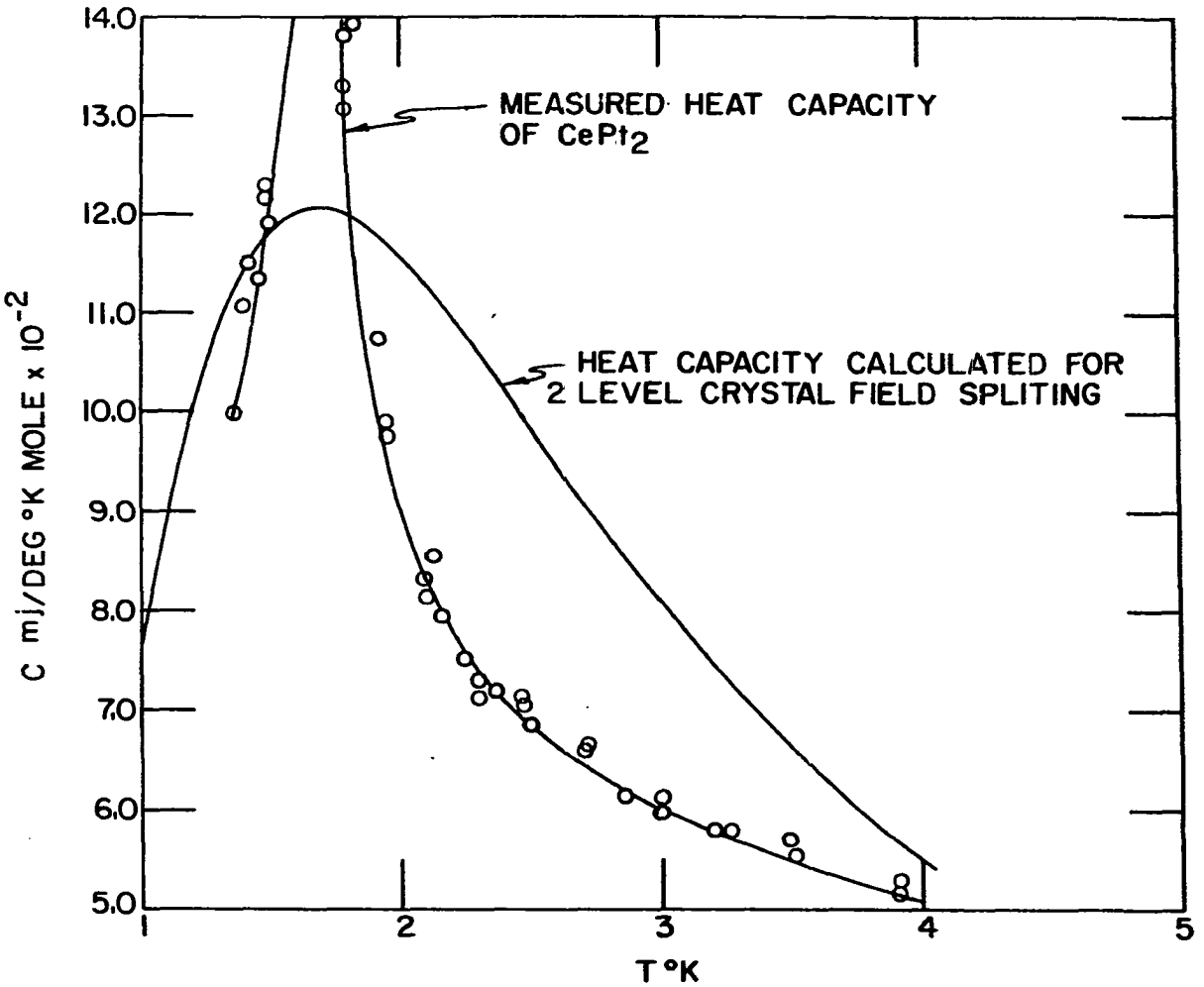


Figure 13. Superimposed Schottky specific heat and measured specific heat of $CePt_2$

The most plausible explanation of the peak in the specific heat is that it is due to magnetic ordering. The application of a field to a material which has a Néel point causes the Néel point of the material to be lowered (30). Also if a material is ordered ferromagnetically the application of field causes the Curie point to occur at a higher temperature. The heat capacity of $CePt_2$ was measured in a field of 9 Koe. As can be seen in Fig. 12 the temperature of the peak shifted slightly downward thus it is concluded that the peak in zero field corresponds to a Néel temperature. Because of the low temperature of the peak it is difficult to determine the nature of the ordering in $CePt_2$ from susceptibility data alone. The reduced moments that have been observed for other $RPt_2$ compounds (31,32) are quite likely to be due to antiferro- or ferri-magnetic ordering.

For the compound $LaPt_2$ the specific heat results are straight forward in that this compound acts like a normal metal (Fig. 14). The specific heat when plotted as C/T versus $T^2$ is a straight line at temperatures below 4.2°K with $\gamma$ = 1.17 ± .02[a] mj/mole $^oK^2$ and $\beta$ = .149 ± .002 mj/mole $^oK^4$ ($\theta_D$ = 236 ± 1°K ). The scatter in this data is somewhat larger than that present in the other data presumably due to the difficulty in obtaining rapid thermal equilibrium with

---

[a]Error limits given by unweighted least squares fit of data.

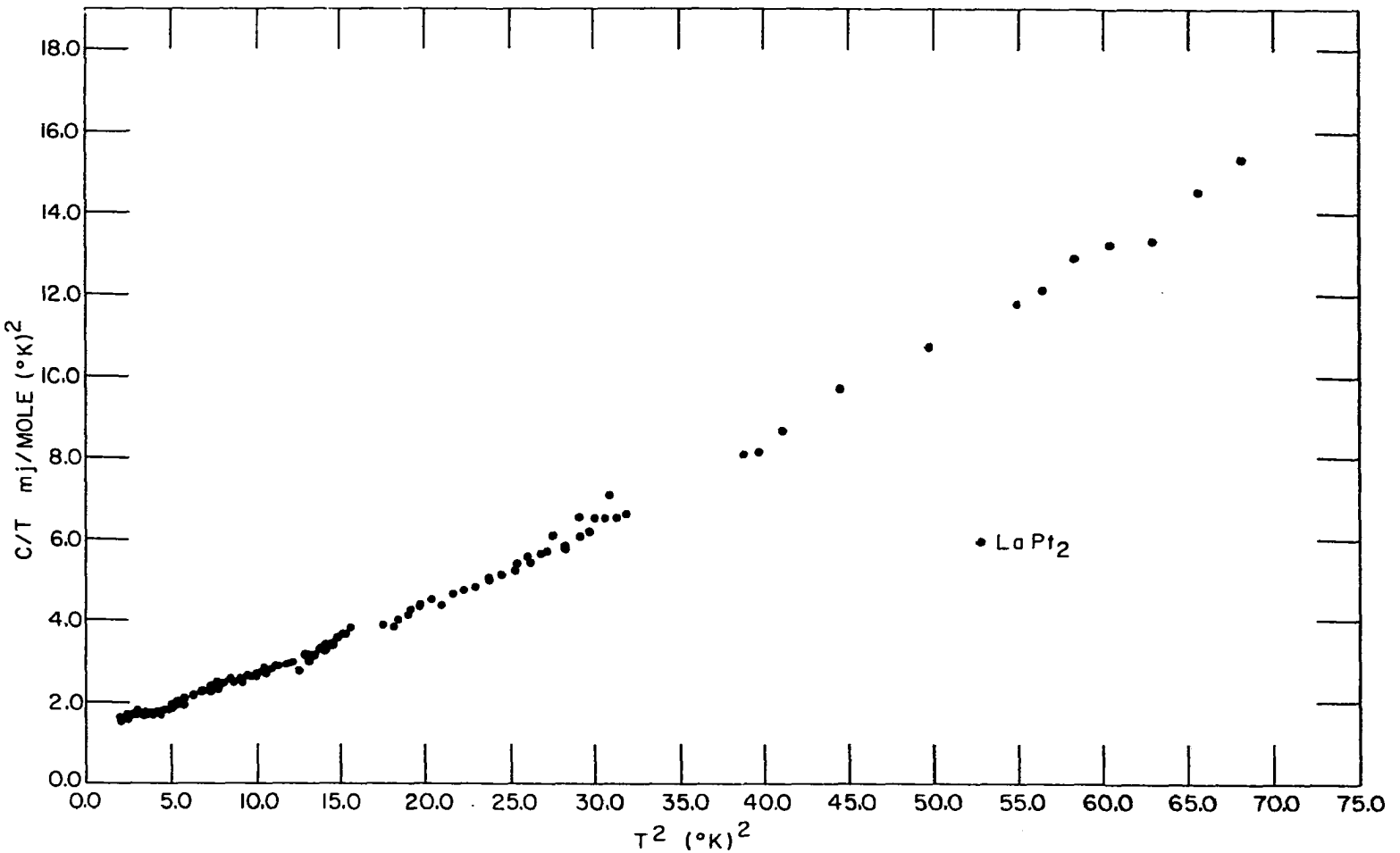


Figure 14. Specific heat of $LaPt_2$

this compound. A higher density of points was taken on this compound to counteract the larger amount of scatter. $LaPt_2$ has been reported to be a superconductor but the reported (33) transition temperature of $0.46^{o}K$ is lower than can be measured with this calorimeter. The low value of $\gamma$ for this compound when compared to the pure elements (La $\gamma = 10.1$ mj/mole $^{o}K^2$ and Pt $\gamma = 6.68$ mj/mole $^{o}K^2$) (34) is not too surprising when it is remembered that the band structure of the compound is expected to be considerably different from that of the pure metals (15).

Figure 12 shows the specific heat data for $LaPt_2$ plotted to the same scale as that of $CePt_2$. It is difficult to draw any conclusions about the $\gamma$ value of $CePt_2$ from the comparison. But if the $\theta_D$ value for $CePt_2$ were much lower than that of $LaPt_2$ the specific heat of $CePt_2$ would have started to rise at the high temperature range of the heat capacity shown in Fig. 12. Instead even at $9^{o}K$ the specific heat is still decreasing from the ordering peak. Thus it appears that $\theta_D$ for $CePt_2$ is at least as large as that measured for $LaPt_2$. Also the $\theta_D$ values for pure cerium and lanthanum are about the same (34) so that it is not expected that $\theta_D$ for the two compounds would be very different. Based on the similarity of constituent atoms, lattice parameter and crystal structure the $\gamma$ value for $CePt_2$ would be expected to have about the same value as that of $LaPt_2$.

Assuming the specific heat curve of $LaPt_2$ represents the electronic and lattice contribution of $CePt_2$ the entropy due to the ordering of $CePt_2$ was determined by extrapolating the C/T versus T curve to zero degrees. Then the lattice and electronic contribution was subtracted off and the area under the curve determined. The entropy was found to be S = R Ln 1.75. This value is much smaller than that predicted for the J = 5/2 ground state, S = R Ln (2J + 1) = R Ln 6.

A possible explanation of this is that crystal field splittings do occur and the splittings are greater than 200 $cm^{-1}$. The ground state would then be expected to be a Kramers doublet. If exchange forces were large enough that ordering did occur the value of the entropy would be S = R Ln 2 which is probably within experimental error of that observed. The fact that the material orders would explain the positive deviation of $1/\chi$ from Curie-Weiss behavior even though crystal field splittings had occurred.

The contribution of the higher levels to the susceptibility at higher temperatures must be such that the 1/T temperature dependence still exists. Because of the experimental problems with low moment samples mentioned before, small deviations of the susceptibility would not have been observed. The high temperature 77-400°K data on $CePt_2$ shows some curvature and an oscillatory behavior of $1/\chi$ versus T (7).

## $LaRu_2$

The only data on the compound $LaRu_2$ that is available in the literature on the electronic or magnetic properties of $LaRu_2$ indicate that it becomes superconducting at 1.63°K (5). Specific heat measurements taken on this compound (Fig. 15) indicate that the transition temperature is about 3°K. If the point where the heat capacity starts to deviate from the high temperature data (35) is taken to be $T_s$ then $T_s$ = 3.20°K. If the midpoint of the transition (36) is taken as $T_s$, then $T_s$ = 3.08. The entropy of the normal and superconducting states should be equal because of the nature of the transformation i.e. 2nd order (37). If $T_s$ is taken as 3.20°K the entropy for the normal and superconducting states are the same. If $T_s$ = 3.08°K is used the entropy in the normal state is 10% larger than that in the superconducting state. The entropy of the superconducting state was calculated assuming no linear term in the heat capacity as has been found for $Nb_3Sn$ (38) and vanadium (39). If a term like this exists for $LaRu_2$ it would cause the entropy in the superconducting state to be somewhat larger. The entropy of the normal state was determined by extrapolating the data for $T > T_s$ to T = 0°K. The value of $\gamma$ was found to be 13.6 $\pm$ .13 mj/mole $^oK^2$, that of $\beta$ to be 0.476 $\pm$ .004 mj/mole $^oK^4$ or $\theta_D$ = 160 $\pm$ 1°K.

It had been hoped initially that a field of 9 Koe would be sufficient to quench superconductivity so that a more

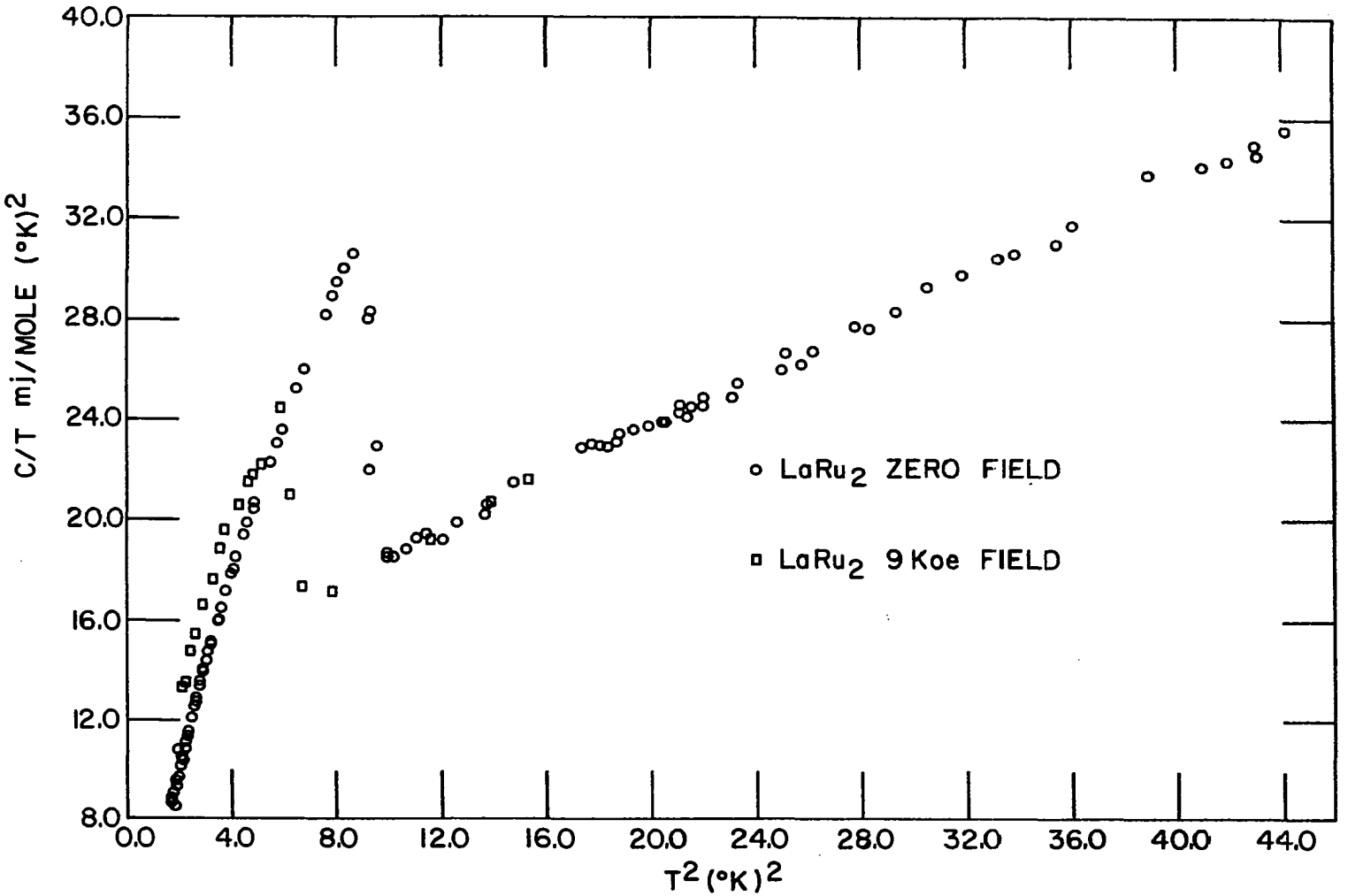


Figure 15. Specific heat of $LaRu_2$

accurate value of $\gamma$ could be determined. Apparently $LaRu_2$ is a type II superconductor with a critical field greater than the thermodynamic critical field. The thermodynamic critical field can be determined from the superconducting specific heat data and a knowledge of the temperature dependence of the critical field. Since the curve separating the superconducting and normal states of a type I superconductor is a true phase boundary (37)

$$G_n - G_s = \frac{VH_c^2}{8\pi} \tag{8}$$

G = Gibbs free energy

$H_c$ = critical field to destroy duperconductivity

V = molar volume

Therefore $\Delta S$ which is the entropy difference is given by

$$\Delta S = S_N - S_S = -\frac{VH_c}{4\pi}\left(\frac{dH_c}{dT}\right)_{T = T_s} \tag{9}$$

The temperature dependence of $H_c$ was originally found experimentally to obey (37)

$$H_c = H_o\left[1 - \left(\frac{T}{T_s}\right)^2\right] \tag{10}$$

where $H_o$ is the critical field at $T = 0^oK$ i.e. the thermodynamic critical field. $H_c$ has been shown by Bardeen, Cooper and Schrieffer (BCS) theory (40) to have the above temperature dependence to within a small error.

For $LaRu_2$ the jump in specific heat at $T_c$ is 44.4 mj/mole $^oK$ using the above value and V = 11.43 cc/mole calcu-

lated from x-ray data.

$$\left(\frac{dH_c}{dT}\right)_{T=T_s} = 385 \text{ oe}/^{o}\text{K} \tag{11}$$

Differentiating Equation 10 and substituting Equation 11 gives the thermodynamic critical field $H_o = 585$ oe.

It can be seen in Fig. 15 that $T_s = 2.49$ $^{o}$K in a field of 9 Koe. A type II superconductor is thought to have two critical fields $H_{c1}$ and $H_{c2}$. $H_{c1}$ is the applied field necessary to prevent the super conductor from being a perfect diamagnet. $H_{c2}$ is the applied field necessary to remove all traces of superconductivity. It is found that $H_{c2}$ can be fit to an equation similar to Equation 10 (39) then using the experimental points $H_{c2}$ can be expressed as

$$H_{c2} = 25{,}700\left[1 - \left(\frac{T}{T_s}\right)^2\right] . \tag{12}$$

It can be seen from the form of this equation that at $0^{o}$K 25.7 Koe is necessary to quench superconductivity.

Recent papers (41,42,43) have dealt with the application of Abrikosovs' theories of type II superconductor. In this theory and its modifications

$$\frac{\Delta C}{T_s(H)} = V\left(\frac{\partial M}{\partial H}\right)_{H_{c2}} \left(\frac{dH_{c2}}{dT}\right)^2 = \frac{V}{4\pi}\, 1.16(2\kappa^2-1) \left(\frac{dH_{c2}}{dT}\right)^2 \tag{13}$$

where $\kappa = \dfrac{H_{c2}}{\sqrt{2}\, H_c}$ near $T_s$. (14)

Using a value of 31 for $\kappa$ as determined from Equation 14 and the other quantities mentioned above a value of $\Delta C = 18.3$ mj/mole $^{o}K$ was derived. This value is only in fair agreement with that determined experimentally of 21.9 mj/mole $^{o}K$. It is thought that the discrepancy partially arises from the lack of data used to determine Equation 12 and also the width of the transition.

$LaRu_2$ seems to be a material which does not obey the BCS theory very well. $\Delta C/\gamma T$ is predicted by BCS theory to be 1.43 but for $LaRu_2$ the value is 1.09. The specific heat of the superconducting electrons was determined by subtracting the lattice contribution from the total specific heat. The data shown in Fig. 16 show that the electrons have a temperature dependent specific heat that is considerably different than that predicted by BCS. The reason for this discrepancy is not known but large differences have been observed for other materials (42).

## $CeRu_2$

Because of the difficulty involved in preparing single phase $CeRu_2$ samples some of the early work on this compound is questionable such as the reported ferromagnetism (44). Also the superconducting transition temperature was originally determined to be $4.9^{o}K$ (5). More recently the value of the transition temperature has been reported as $6.01 \pm .15^{o}K$ (8). This value is in close agreement with the value

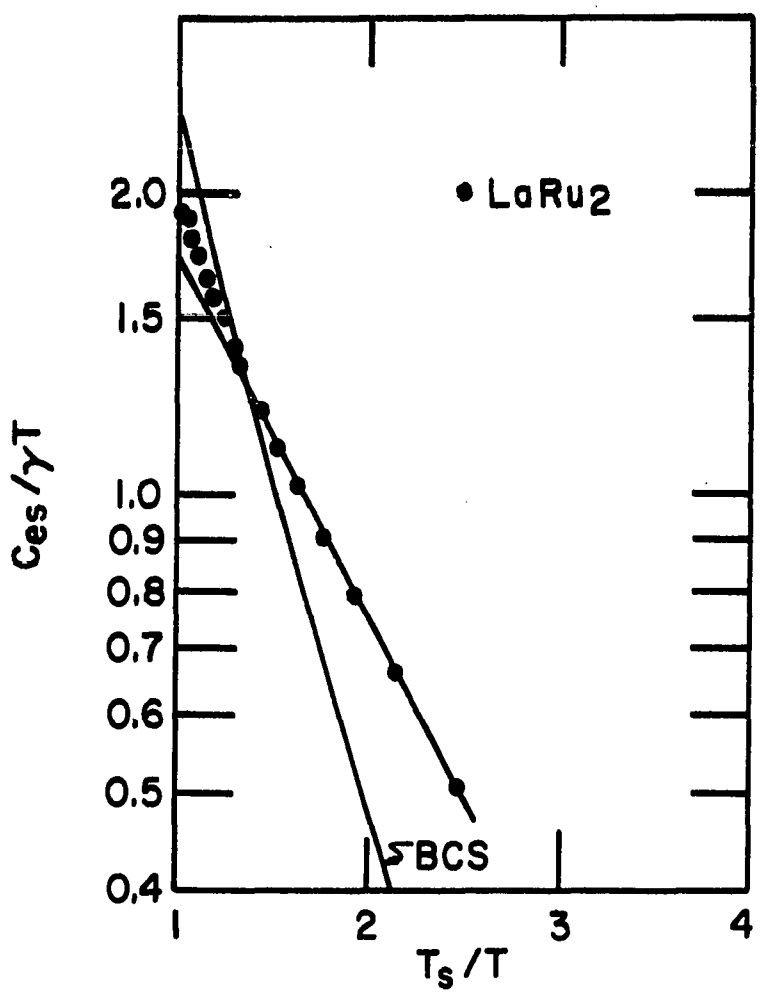


Figure 16. The specific heat of the superconducting electrons in $LaRu_2$ versus reduced temperature

($T_s$ = 5.92°K) determined from the specific heat data taken on this compound (Fig. 17). The magnetic susceptibility of this compound measured in the range 77°K to 473°K has been reported to be temperature independent (7).

From the specific heat data above the transition temperature the value of $\gamma$ and $\theta_D$ were determined to be 23.3 ± .61 mj/mole $^oK^2$ and 171°K ± 2 respectively. It was found that the entropy of the normal state was 20 percent larger than that in the superconducting state. This anomaly is comparable to that found in $Nb_3Sn$ (42). The discrepancy in $Nb_3Sn$ was attributed to the difficulty in determining the normal state specific heat. Large enough magnetic fields are not available to quench the superconductivity so that normal state behavior has to be inferred from the data above the transition. For the case of $Nb_3Sn$ it was thought that the normal Debye extrapolation was incorrect and that the $\gamma$ value was about half of that predicted from the extrapolation and that the $\theta_D$ increased about 1°K/°K. $\gamma$ and $\theta_D$ can be determined for $CeRu_2$ in such a way that the entropy is equal and the heat capacity above the transition is the same. The values determined this way are $\gamma$ = 13.3 mj/mole $^oK^2$ $\theta_D$ = 144°K. It is not clear that the above analysis should be applied to $CeRu_2$ and other possible explanations which are more plausible will be mentioned later.

The specific heat of $CeRu_2$ has been measured in field of 2,4,6,9 Koe to determine the behavior of the superconducting

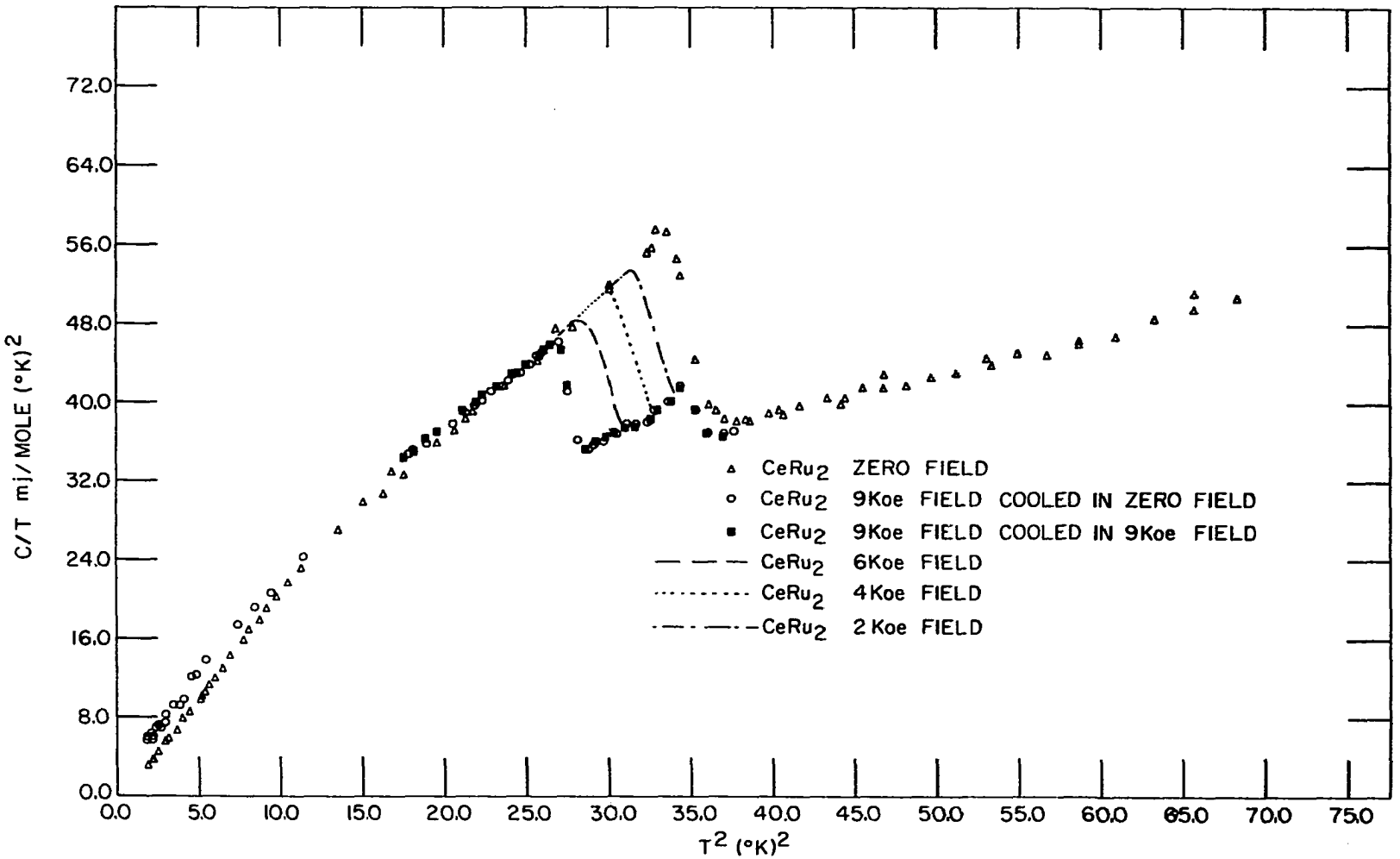


Figure 17. Specific heat of $CePt_2$

transitions in various fields. It is clear from the specific heat data that $CeRu_2$ is a type II superconductor. The thermodynamic critical field determined from an analysis similar to that of $LaRu_2$ is 1.53 Koe and $H_{c2}$ at $0^oK$ is 40 Koe.

It can be seen from Fig. 17 that the specific heat of $CeRu_2$ in a field shows a bump occurring at about the same temperature as the transition in zero field. The bump appears to be independent of field with respect to magnitude and temperature. The origin of this bump is not clear. It does not seem likely that an impurity phase would cause an anomaly right at the superconducting transition of $CeRu_2$. Also if this anomaly occurred in zero field the transition might be expected to be broader than it is. The possibility of such an impurity contribution can not be ruled out particularly since 1.8 percent of cerium rich cerium-ruthenium alloy is present in addition to the 2 percent inclusions. Also an impurity phase being present could account for the difference in entropy observed between the two states. To determine whether or not the specific heat in the region of the bump depended upon sample history the specific heat was measured after the sample had been cooled through its transition in 9 Koe. As the data in Fig. 17 show there is no difference between these results and those obtained when the sample is cooled in zero field. Thus the heat capacity of a sample appears to be completely reversible in a magnetic field

indicating no flux traping.

It is difficult to assess the effect of the 1.8 percent of cerium rich Ce-Ru alloy without knowing some of its electrical and magnetic properties. If the alloy is magnetic as is β cerium the effect could be large and might explain the entropy anomaly. If the alloy were superconducting with a higher transition temperature than $CeRu_2$ the anomaly in the magnetic field might be explained by assuming shielding of some of the $CeRu_2$ with a superconducting sheath. It is clear that the results for $CeRu_2$ have been clouded by not knowing what effect, if any, the 1.8 percent of the extra phase present has on the anomalous behavior observed for $CeRu_2$.

## SUMMARY

The low temperature properties of the Laves phase compounds $CePt_2$, $CeRu_2$, $LaPt_2$, and $LaRu_2$ have been measured. One of the interesting results of this investigation has been the observation that both of the ruthenium compounds have large values of $\gamma$ and values of $\theta_D$ near those of the rare earth metal. The value of $\theta_D$ for $LaPt_2$ has been measured and found to be close to the $\theta_D$ for platinum. Also $\theta_D$ for $CePt_2$ has been inferred, by comparing the specific heats of $LaPt_2$ and $CePt_2$, to be not much smaller, if any, than that for $LaPt_2$. Thus it appears that for the ruthenium compounds it is the rare earth atoms which are giving the lattice its rigidity i.e. rare earth-rare earth contacts and in the case of the platinum compounds it is the transition metals.

The value $r_A{}^{cal}/r_B$ (Table 2) for the platinum compounds is somewhat less than ideal, 1.208 versus 1.225. And as was described earlier, for radius ratios less than ideal, B atom contacts occur thus explaining why the platinum compounds have $\theta_D$ values more like the pure B atoms. In the case of the ruthenium compound Table 2 shows that the radius ratios are 1.244 and 1.219 for lanthanum and cerium respectively. Thus these values are about the same as the ideal or slightly larger thus making it plausible that in these compounds the elastic constants are controlled by A-A contacts in agreement with the specific heat data.

To ascertain whether or not the behavior of the $\theta_D$ described above holds just for these compounds or is general for Laves phases Table 5 was prepared which lists $\theta_D$ for the Laves phases in comparison with $\theta_D$ for the pure components. It can be seen that in all cases if $r^{cal}/r_B$ is considerably less than theoretical then $\theta_D$ for the compound is closer to $\theta_D$ for the pure B element than for the A element. If $r^{cal}/r_B$ is approximately equal or greater than ideal then $\theta_D$ for the compound is closer to $\theta_D$ for the A element. Considering that there are over 280 known Laves phase compounds the sampling statistics here are not very good but this is apparently all the data available. The agreement between the Debye temperature of $MgCu_2$ measured calorimetrically and by elastic constants gives some confidence that the calorimetric determined Debye temperature is a measure of the forces holding the atoms together in these compounds.

The fact that the $\gamma$ values of the ruthenium compounds are large compared to $LaPt_2$ indicates that large band structure effects occur in these compounds which if sufficient information were available might serve to explain the order of the compounds in Table 1.

Table 5. Comparison of Debye temperatures for Laves phases and their components

| Compound | $r_A/r_B$ | $r^{cal}/r_B$ | $\theta_{cal}$[a] | $\theta_{EL}$[b] | $\theta_A(34)$ | $\theta_B(34)$ |
|---|---|---|---|---|---|---|
| | | Compounds with $r^{cal}/r_B$ less than ideal | | | | |
| $ZrCo_2$ C15 | 1.280 | 1.203 | | 420[c] | 289 | 452 |
| $HfCo_2$ C15 | 1.262 | 1.197 | 3 | 368[c] | 256 | 452 |
| $MgCu_2$ C15 | 1.253 | 1.194 | 332(15) | 336.4[d] | 396 | 342 |
| $LaPt_2$ C15 | 1.353 | 1.209 | 238 | | 142 | 234 |
| $CaMg_2$ C14 | 1.232 | 1.184 | | 425.5[e] | 234 | 396 |
| | | Compounds with $r^{cal}/r_B$ ideal | | | | |
| $CeNi_2$ C15 | 1.482 | 1.224 | 227(45) | | 146[f] | 427 |
| $CeRu_2$ C15 | 1.379 | 1.219 | 171 | | 146[f] | 600 |
| $LaRu_2$ C15 | 1.402 | 1.244 | 160 | | 142 | 600 |

[a]$\theta_{cal}$ = Debye temperature from specific heat data.

[b]$\theta_{EL}$ = Debye temperature from elastic constant data.

[c]G. W. Shannette, Ames Laboratory, Ames, Iowa. Debye $\theta$ of $ZrCo_2$ and $HfCo_2$. Private communications. 1968.

[d]Calculated from elastic constants at 80°K by G. W. Shannette, Ames Laboratory, Ames, Iowa from Ref. 46.

[e]Calculated from elastic constants at 100°K by G. W. Shannette, Ames Laboratory, Ames, Iowa from Ref. 47.

[f]The value for $Ce^{+3}$ is used here. A value of $Ce^{+4}$ can be estimated from the Lindemann equation (34)

$$\theta^M = K(T_m/M)^{\frac{1}{2}}(1/V)^{1/3}$$

if the melting point ($T_m$) of $Ce^{+4}$ can be estimated. $T_m$ of $Ce^{+4}$ was approximated from $T_m$ of $Ce^{+3}$ and the difference in melting point between lutetium (+3) and hafnium (+4). The value of $\theta_M$ so determined was 239°K. It is expected that the value is probably high so that $\theta_D$ for $Ce^{+4}$ falls between the values 146°K and 239°K.

## ACKNOWLEDGEMENTS

I am very much indebted to many people around the Ames Laboratory for the many discussions and ideas they have contributed to this thesis. I wish to pick out a few for special acknowledgement: Dr. D. K. Finnemore for the many helpful discussions on superconductivity and the loan of his calibrated germanium resistance thermometer; B. J. Beaudry and P. E. Palmer for the preparation of the rare earth metals; F. A. Schmidt for the aid in preparing the arc zone melted compounds; Drs. A. E. Miller and W. J. Gray for the construction of the vibrating sample magnetometer; G. W. Shannette for the use of some of his unpublished data; Dr. V. A. Fassel and F. Laabs for the analytical work including the x-ray microprobe analysis; T. C. Cetas for writing some of the computer programs used. I most certainly wish to express my gratitude and thanks to Dr. K. A. Gschneidner, Jr. for suggesting this problem and for the continued support and encouragement he has given during the course of this work.

Last but not least I wish to express my thanks to my wife and children for their willingness to undergo numerous sacrifices so that this thesis could be completed.

# BIBLIOGRAPHY


1. Gschneidner, K. A., Jr., Elliott, R. O. and McDoanld, R. R. J. Phys. Chem. Solids 23, 555 (1962).

2. Schuch, A. F. and Sturdivant, J. H., J. Chem. Phys. 18, 145 (1950).

3. Lawson, A. W. and Tang, T. Phys. Rev. 76, 301 (1949).

4. Gschneidner, K. A., Jr. and Smoluchowski, R. J. Less Common Metals 5, 374 (1963).

5. Matthias, B. T., Suhl, H. and Corenzwit, E. Phys. Rev. Letters 1, 92 (1958).

6. Gschneidner, K. A., Jr. Rare Earth Alloys. Van Nostrand, Princeton, New Jersey (1961).

7. Olcese, G. L. Boll. Sci. Chim. Inc., Bologna 24, 165 (1966). Original available but not translated; translated in U.S. Atomic Energy Commission Report, IS-Trans-70 [Iowa State University, Ames, Inst. for Atomic Research]. 1967.

8. Smith, T. F. and Harris, I. R. J. Phys. Chem. Solids, 28, 1846 (1967).

9. Williams, H. J., Wernick, J. H., Neasbit, E. A. and Sherwood, R. C. J. Phys. Soc. Japan 17, 19 (1962).

10. Wertheim, G. K. and Wernick, J. H. Phys. Rev. 125, 1937 (1962).

11. Hume-Rothery, W. and Raynor, G. V. The Structure of Metals and Alloys, the Institute of Metals, London, England (1962).

12. Schulze, G. E. R. Z. Krist. 111, 249 (1959).

13. Rosenberg, H., Low Temperature Solid State Physics, Oxford University press, London, England, 1963.

14. Gopal, E. S. R., Specific Heats at Low Temperatures, Plenum Press, New York, New York, 1966.

15. Slick, P. I., Massena, C. W. and Craig, R. S. J. Chem. Phys. 43, 2788 (1965).

16. Heiniger, F., Bucher, E., Muller, J., Phys. Kondens. Materie 5, 243 (1966).

17. Obrowski, W. Z. Metallk. 53, 736 (1962).

18. Carlson, O. N., Schmidt, F. A. and Paulson, W. M. Transactions American Society for Metals 57, 356 (1964).

19. Dwight, A. Transactions American Society for Metals 53, 479 (1961).

20. Dwight, A. E., Conner, R. A. and Downey, J. W. Acta Cryst. 18, 835 (1965).

21. Sterling, H. F. and Warren, R. W. Metallurgia 67, 301 (1963).

22. Schob, O. B. and Parthe', E. Acta Cryst. 19, 214 (1965).

23. Neighbor, J. E. Rev. Sci. Inst. 37, 497 (1966).

24. Catland, G. and Plump, H. Journal of Research U.S. Bureau of Standards 70A, 243 (1966).

25. Finnemore, D. K., Johnson, D. L., Ostenson, J. E. Spedding, F. H. and Beaudry, B. J. Phys. Rev. 137, 550 (1965).

26. Rogers, J. S., Tanish, R. J., Anderson, M. S. and Swenson, C. E. Comparison between Gas Thermometer, Acoustic, and Platinum Resistance Temperature Scales between 2 and 20°K. Metrogolia [to be published 1968].

27. Brickwedde, F. G., van Dijk, H. Durieux, M., Clement, J. R. and Logan, J. K. Journal of Research U.S. National Bureau of Standards 64A, 1 (1960).

28. Osborne, D. W., Flotow, H. E. and Schreiner, F., Rev. Sci. Instr. 38, 159 (1967).

29. Miller, A. E. U.S. Atomic Energy Commission Rept., IS-1717, Ames Laboratory, [Iowa State University, Ames, Inst. for Atomic Research], Ca. 1968.

30. Gray, W. J. The Magnetic Properties of Single Crystals of Erbium and Some Yttrium-Erbium and Lutetium-Erbium Alloys between 1.2 and 300°K, Unpublished Ph.D. thesis, Library, Iowa State University of Science and Technology, Ames, Iowa. 1968.

31. Wallace, W. E. and Vlasov, Y. G. Inorg. Chem. 6, 2216 (1967).

32. Crangle, J. and Ross, J. W. Proc. Intern. Conf. Magnetism Nottingham, Sept. 1964, Institute of Physics, London, England, 1965.

33. Geballe, T. H., Matthias, B. T., Compton, V. B., Corenzwit, E., Hull, G. W., Jr. and Longinotti, L. D. Phys. Rev. 137, 119 (1965).

34. Gschneidner, K. A., Jr. Solid State Physics 16, 276 (1964).

35. Geballe, T. H., Matthias, B. T., Remeika, J. P., Clogston, A. M., Compton, V. B., Maita, J. P. and Williams, H. J. Physics 22, 293 (1966).

36. Johnson, D. and Finnemore, D., Phys. Rev. 158, 376 (1967).

37. Shoenberg, D., Superconductivity. Cambridge University Press, London, England, 1960.

38. Vieland, L. and Wieklund, A. W. Phys. letters 23, 223 (1966).

39. Radebaugh, R. and Keesom, P. Phys. Rev. 149, 209 (1966).

40. Bardeen, J., Cooper, L. M. and Schrieffer, J. R. Phys. Rev. 108, 1175 (1957).

41. Hake, R. R. and Brammer, W. G., Phys. Rev. 133, 719 (1964).

42. Vieland, L. J. and Wicklund, A. Phys. Rev. 166, 424 (1968).

43. McConville, T. and Serin, B. Phys. Rev. 140, 1169 (1965).

44. Bozorth, R. M., Matthias, B. T., Suhl, H., Corenzwit, E. and Davis, D. D. Phys. Rev. 115, 1595 (1959).

45. Dixon, M., Aoyagi, M., Craig, R. S., and Wallace, W. E. Crystal Field Heat Capacities of $PrNi_2$ and PrBi. Unpublished paper presented at 6th Rare Earth Research Conference, Gatlinburg, Tenn. 1967. Conference preprint Chemistry Dept. Univ. of Pittsburg, Pittsburg, Pa. 1967.

46. Cheng, C. H. J. Phys. Chem. Solids 28, 413 (1967).

47. Sumer, A. and Smith, J. F. J. Appl. Phys. 38, 2283 (1962).

# APPENDIX

Table A1. Specific heat of copper standard

| $\frac{C}{T}$ $\frac{mJoule}{mole\ {}^oK^2}$ | $T^2\ {}^oK^2$ | $\frac{C}{T}$ $\frac{mJoule}{mole\ {}^oK^2}$ | $T^2\ {}^oK^2$ | $\frac{C}{T}$ $\frac{mJoule}{mole\ {}^oK^2}$ | $T^2\ {}^oK^2$ |
|---|---|---|---|---|---|
| 0.742 | 2.050 | 1.07 | 7.563 | 1.80 | 24.229 |
| 0.792 | 2.113 | 1.06 | 7.832 | 1.89 | 26.254 |
| 0.801 | 2.312 | 1.09 | 8.232 | 2.03 | 28.163 |
| 0.821 | 2.380 | 1.11 | 8.657 | 2.13 | 30.549 |
| 0.830 | 2.657 | 1.16 | 9.235 | 2.32 | 34.452 |
| 0.815 | 2.704 | 1.21 | 9.824 | 2.42 | 36.886 |
| 0.838 | 2.948 | 1.20 | 10.621 | 2.62 | 40.262 |
| 0.834 | 3.271 | 1.32 | 12.060 | 2.97 | 46.293 |
| 0.861 | 3.440 | 1.31 | 13.661 | 3.22 | 53.037 |
| 0.858 | 3.815 | 1.33 | 14.356 | 3.35 | 54.603 |
| 0.876 | 4.075 | 1.52 | 17.459 | 3.38 | 56.247 |
| 0.900 | 4.317 | 1.54 | 18.148 | 3.50 | 58.811 |
| 0.943 | 5.412 | 1.66 | 20.247 | 3.89 | 66.074 |
| 0.984 | 6.004 | 1.71 | 22.680 | 4.30 | 71.924 |

Table A2. Specific heat of $CePt_2$ zero field

| $\frac{C}{T}$ $\frac{mJoule}{mole\ {}^oK^2}$ | $T^2\ {}^oK^2$ | $\frac{C}{T}$ $\frac{mJoule}{mole\ {}^oK^2}$ | $T^2\ {}^oK^2$ | $\frac{C}{T}$ $\frac{mJoule}{mole\ {}^oK^2}$ | $T^2\ {}^oK^2$ |
|---|---|---|---|---|---|
| $73.9 \times 10^1$ | 1.853 | $36.7 \times 10^1$ | 4.679 | $13.2 \times 10^1$ | 14.240 |
| 77.6 | 1.885 | 33.4 | 5.100 | 12.5 | 16.621 |
| 79.5 | 1.952 | 31.5 | 5.363 | 11.8 | 17.113 |
| 81.1 | 2.002 | 31.1 | 5.570 | 10.9 | 18.364 |
| 79.1 | 2.055 | 29.2 | 5.988 | 9.90 | 20.834 |
| 82.8 | 2.121 | 26.9 | 6.273 | 9.33 | 22.693 |
| 83.4 | 2.160 | 23.1 | 7.657 | 8.46 | 25.961 |
| 95.9 | 2.451 | 21.4 | 8.232 | 7.42 | 30.078 |
| 117. | 2.796 | 20.4 | 9.078 | 6.72 | 37.020 |
| 90.1 | 2.950 | 19.6 | 9.270 | 6.14 | 38.730 |
| 74.8 | 3.168 | 18.6 | 9.758 | 5.71 | 41.966 |
| 77.2 | 3.230 | 19.2 | 10.186 | 4.73 | 52.784 |
| 76.7 | 3.315 | 18.0 | 10.313 | 4.67 | 55.005 |
| 49.9 | 3.808 | 17.8 | 10.534 | 4.45 | 59.157 |
| 54.8 | 3.833 | 17.8 | 10.638 | 4.08 | 68.652 |
| 47.3 | 3.954 | 17.8 | 10.699 | 3.66 | 82.817 |
| 39.4 | 4.476 | 15.7 | 12.483 | | |

Table A3. Specific heat of $CePt_2$ 9.0 Koe field

| $\frac{C}{T}$ $\frac{mJoule}{mole\ {}^oK^2}$ | $T^2\ {}^oK^2$ | $\frac{C}{T}$ $\frac{mJoule}{mole\ {}^oK^2}$ | $T^2\ {}^oK^2$ | $\frac{C}{T}$ $\frac{mJoule}{mole\ {}^oK^2}$ | $T^2\ {}^oK^2$ |
|---|---|---|---|---|---|
| $7.49 \times 10^2$ | 1.987 | $7.66 \times 10^2$ | 2.661 | $3.69 \times 10^2$ | 4.938 |
| 7.45 | 2.050 | 7.60 | 2.696 | 3.50 | 5.177 |
| 7.68 | 2.113 | 7.63 | 2.740 | 3.30 | 5.452 |
| 7.57 | 2.138 | 7.40 | 2.774 | 3.17 | 5.784 |
| 7.69 | 2.178 | 7.32 | 2.791 | 3.01 | 6.154 |
| 7.66 | 2.186 | 7.39 | 2.846 | 2.44 | 8.252 |
| 7.74 | 2.244 | 7.19 | 2.891 | 2.32 | 8.816 |
| 7.92 | 2.314 | 7.17 | 2.963 | 2.18 | 9.457 |
| 7.82 | 2.405 | 6.70 | 3.016 | 2.05 | 10.086 |
| 7.73 | 2.481 | 6.44 | 3.119 | 1.94 | 10.695 |
| 7.74 | 2.509 | 5.98 | 3.209 | 1.58 | 14.361 |
| 7.74 | 2.563 | 5.68 | 3.300 | 1.44 | 15.042 |
| 7.66 | 2.603 | 5.28 | 3.395 | 1.48 | 15.738 |
| 7.58 | 2.651 | 4.46 | 3.971 | | |

Table A4. Specific heat of $LaPt_2$ zero field

| $\frac{C}{T}$ $\frac{mJoule}{mole\ {}^oK^2}$ | $T^2 {}^oK^2$ | $\frac{C}{T}$ $\frac{mJoule}{mole\ {}^oK^2}$ | $T^2 {}^oK^2$ | $\frac{C}{T}$ $\frac{mJoule}{mole\ {}^oK^2}$ | $T^2 {}^oK^2$ |
|---|---|---|---|---|---|
| 1.52 | 2.030 | 2.31 | 7.843 | 4.29 | 19.751 |
| 1.57 | 2.064 | 2.43 | 8.239 | 4.39 | 19.851 |
| 1.54 | 2.148 | 2.53 | 8.590 | 4.49 | 20.447 |
| 1.56 | 2.187 | 2.50 | 8.783 | 4.36 | 21.055 |
| 1.57 | 2.287 | 2.55 | 9.213 | 4.64 | 21.681 |
| 1.59 | 2.334 | 2.46 | 9.286 | 4.70 | 22.281 |
| 1.61 | 2.435 | 2.62 | 9.575 | 4.79 | 23.073 |
| 1.66 | 2.479 | 2.63 | 9.762 | 5.01 | 23.806 |
| 1.69 | 2.637 | 2.65 | 9.823 | 4.96 | 23.854 |
| 1.65 | 2.824 | 2.68 | 10.109 | 5.09 | 24.563 |
| 1.69 | 2.834 | 2.61 | 10.111 | 5.10 | 24.591 |
| 1.65 | 3.003 | 2.74 | 10.430 | 5.20 | 25.397 |
| 1.76 | 3.025 | 2.84 | 10.625 | 5.34 | 25.494 |
| 1.67 | 3.194 | 2.67 | 10.738 | 5.53 | 26.151 |
| 1.69 | 3.409 | 2.79 | 10.071 | 5.40 | 26.304 |
| 1.64 | 3.415 | 2.87 | 11.287 | 5.59 | 26.892 |
| 1.73 | 3.539 | 2.89 | 11.482 | 5.66 | 27.267 |
| 1.66 | 3.621 | 2.91 | 11.914 | 6.03 | 27.617 |
| 1.66 | 3.889 | 2.94 | 12.168 | 5.79 | 28.318 |
| 1.71 | 3.933 | 2.96 | 12.286 | 5.73 | 28.358 |
| 1.74 | 4.259 | 2.75 | 12.671 | 6.02 | 29.188 |
| 1.65 | 4.467 | 3.10 | 13.073 | 6.49 | 29.211 |
| 1.76 | 4.679 | 2.97 | 13.246 | 6.11 | 29.761 |
| 1.78 | 4.719 | 3.11 | 13.620 | 6.48 | 30.009 |
| 1.82 | 4.910 | 3.25 | 13.917 | 6.46 | 30.068 |
| 1.84 | 4.996 | 3.21 | 13.974 | 7.03 | 30.097 |
| 1.86 | 5.133 | 3.23 | 14.197 | 6.48 | 31.395 |
| 1.89 | 5.291 | 3.35 | 14.269 | 6.55 | 31.957 |
| 1.97 | 5.423 | 3.36 | 14.633 | 8.11 | 38.685 |
| 1.91 | 5.458 | 3.39 | 14.635 | 8.10 | 39.682 |
| 1.92 | 5.833 | 3.55 | 14.945 | 8.62 | 41.087 |
| 2.07 | 5.909 | 3.65 | 15.269 | 9.67 | 44.506 |
| 2.14 | 6.379 | 3.64 | 15.428 | 10.6 | 49.723 |
| 2.26 | 6.894 | 3.80 | 15.689 | 11.7 | 54.934 |
| 2.29 | 6.998 | 3.87 | 17.590 | 12.1 | 56.461 |
| 2.24 | 7.073 | 3.82 | 18.268 | 12.8 | 58.306 |
| 2.36 | 7.406 | 3.97 | 18.493 | 13.2 | 60.330 |
| 2.23 | 7.474 | 4.11 | 19.099 | 13.3 | 62.889 |
| 2.46 | 7.780 | 4.23 | 19.256 | 14.5 | 65.525 |
| | | | | 15.3 | 68.167 |

Table A5. Specific heat of $LaRu_2$ zero field

| $\frac{C}{T}$ $\frac{mJoule}{mole\ {}^oK^2}$ | $T^2 {}^oK^2$ | $\frac{C}{T}$ $\frac{mJoule}{mole\ {}^oK^2}$ | $T^2 {}^oK^2$ | $\frac{C}{T}$ $\frac{mJoule}{mole\ {}^oK^2}$ | $T^2 {}^oK^2$ |
|---|---|---|---|---|---|
| 8.67 | 1.621 | 17.8 | 3.949 | 23.3 | 18.754 |
| 8.86 | 1.648 | 18.4 | 4.147 | 23.4 | 19.267 |
| 8.80 | 1.673 | 19.3 | 4.482 | 23.6 | 19.821 |
| 9.10 | 1.732 | 19.8 | 4.608 | 23.8 | 20.391 |
| 9.00 | 1.746 | 20.5 | 4.829 | 23.8 | 20.534 |
| 8.56 | 1.792 | 20.3 | 4.852 | 24.2 | 20.981 |
| 9.54 | 1.846 | 21.2 | 5.488 | 24.5 | 21.095 |
| 9.32 | 1.850 | 22.9 | 5.705 | 24.2 | 21.098 |
| 10.8 | 1.883 | 23.4 | 5.934 | 24.0 | 21.277 |
| 9.67 | 1.908 | 25.1 | 6.492 | 24.3 | 21.465 |
| 10.5 | 2.021 | 25.9 | 6.811 | 24.4 | 21.930 |
| 10.1 | 2.025 | 28.1 | 7.615 | 24.8 | 21.940 |
| 10.3 | 2.068 | 28.8 | 7.822 | 24.8 | 23.026 |
| 10.4 | 2.102 | 29.4 | 8.034 | 25.4 | 23.239 |
| 10.8 | 2.168 | 29.9 | 8.276 | 25.9 | 24.905 |
| 11.1 | 2.214 | 30.5 | 8.634 | 26.6 | 25.080 |
| 11.3 | 2.278 | 28.0 | 9.220 | 26.1 | 25.666 |
| 11.5 | 2.311 | 28.7 | 9.298 | 26.6 | 26.129 |
| 12.0 | 2.406 | 22.8 | 9.510 | 27.6 | 27.717 |
| 12.1 | 2.441 | 18.6 | 9.903 | 27.6 | 28.294 |
| 12.5 | 2.508 | 18.5 | 9.957 | 28.2 | 29.334 |
| 12.7 | 2.565 | 18.4 | 10.122 | 29.2 | 30.525 |
| 12.8 | 2.609 | 18.7 | 10.624 | 29.7 | 31.792 |
| 13.3 | 2.703 | 19.2 | 11.031 | 30.4 | 33.179 |
| 13.5 | 2.737 | 19.3 | 11.424 | 30.5 | 33.810 |
| 14.0 | 2.878 | 19.1 | 12.048 | 30.9 | 35.389 |
| 13.9 | 2.880 | 19.8 | 12.591 | 31.6 | 35.999 |
| 14.3 | 2.986 | 20.1 | 13.626 | 33.7 | 38.870 |
| 14.7 | 3.047 | 20.5 | 13.757 | 34.0 | 40.906 |
| 15.1 | 3.188 | 21.4 | 14.771 | 34.2 | 41.886 |
| 15.2 | 3.213 | 22.8 | 17.319 | 34.8 | 42.975 |
| 15.9 | 3.439 | 22.9 | 17.663 | 34.4 | 42.027 |
| 16.0 | 3.466 | 22.8 | 18.024 | 35.4 | 44.158 |
| 16.4 | 3.596 | 22.8 | 18.306 | | |
| 17.1 | 3.741 | 23.0 | 18.621 | | |

Table A6. Specific heat of $LaRu_2$ 9.0 Koe field

| $\frac{C}{T}$ $\frac{mJoule}{mole\ {}^oK^2}$ | $T^2 {}^oK^2$ | $\frac{C}{T}$ $\frac{mJoule}{mole\ {}^oK^2}$ | $T^2 {}^oK^2$ | $\frac{C}{T}$ $\frac{mJoule}{mole\ {}^oK^2}$ | $T^2 {}^oK^2$ |
|---|---|---|---|---|---|
| 13.5 | 2.039 | 17.8 | 3.157 | 24.6 | 5.895 |
| 13.6 | 2.171 | 18.9 | 3.604 | 17.4 | 6.790 |
| 14.4 | 2.258 | 19.6 | 3.853 | 17.1 | 7.943 |
| 14.9 | 2.400 | 20.7 | 4.294 | 19.1 | 11.568 |
| 15.8 | 2.555 | 22.0 | 4.708 | 20.9 | 13.873 |
| 16.8 | 2.857 | 23.0 | 5.220 | 21.9 | 15.100 |

Table A7. Specific heat of $CeRu_2$ zero field

| $\frac{C}{T}$ $\frac{mJoule}{mole\ {}^oK^2}$ | $T^2 {}^oK^2$ | $\frac{C}{T}$ $\frac{mJoule}{mole\ {}^oK^2}$ | $T^2 {}^oK^2$ | $\frac{C}{T}$ $\frac{mJoule}{mole\ {}^oK^2}$ | $T^2 {}^oK^2$ |
|---|---|---|---|---|---|
| 3.12 | 1.941 | 27.0 | 13.602 | 38.3 | 38.413 |
| 3.68 | 2.187 | 29.8 | 15.151 | 38.1 | 38.656 |
| 3.67 | 2.317 | 30.6 | 16.344 | 38.9 | 39.799 |
| 4.55 | 2.545 | 33.0 | 16.846 | 39.2 | 40.430 |
| 5.59 | 2.970 | 32.5 | 17.569 | 38.7 | 40.697 |
| 5.67 | 3.088 | 35.8 | 19.672 | 39.6 | 41.714 |
| 6.58 | 3.634 | 37.1 | 20.702 | 40.4 | 43.421 |
| 7.70 | 4.064 | 38.3 | 21.373 | 39.7 | 44.247 |
| 8.51 | 4.471 | 39.0 | 21.819 | 40.4 | 44.499 |
| 8.55 | 4.503 | 41.7 | 23.806 | 41.5 | 45.583 |
| 9.96 | 5.133 | 41.9 | 23.842 | 41.4 | 46.837 |
| 9.88 | 5.138 | 44.2 | 25.717 | 42.9 | 46.913 |
| 10.1 | 5.257 | 47.7 | 26.866 | 41.7 | 48.238 |
| 10.4 | 5.389 | 47.7 | 27.884 | 42.6 | 49.684 |
| 11.2 | 5.675 | 51.4 | 30.139 | 43.1 | 51.219 |
| 12.0 | 6.017 | 51.8 | 30.148 | 44.5 | 53.073 |
| 12.9 | 6.484 | 55.2 | 32.429 | 43.9 | 53.399 |
| 14.2 | 6.993 | 55.6 | 32.756 | 44.9 | 56.757 |
| 15.8 | 7.785 | 57.5 | 33.012 | 46.1 | 58.694 |
| 16.9 | 8.172 | 57.3 | 33.670 | 46.3 | 58.734 |
| 17.7 | 8.731 | 54.6 | 34.258 | 46.7 | 60.893 |
| 18.9 | 9.205 | 52.9 | 34.449 | 48.5 | 63.301 |
| 20.1 | 9.797 | 44.3 | 35.367 | 49.5 | 65.627 |
| 20.1 | 9.869 | 39.7 | 36.212 | 51.1 | 65.755 |
| 21.5 | 10.534 | 39.2 | 36.582 | 50.7 | 68.369 |
| 23.0 | 11.329 | 38.3 | 37.079 | | |
| 27.0 | 13.563 | 38.1 | 37.862 | | |

Table A8. Specific heat of $CeRu_2$ 2.0 Koe field

| $\frac{C}{T}$ $\frac{mJoule}{mole\ ^oK^2}$ | $T^2\ ^oK^2$ | $\frac{C}{T}$ $\frac{mJoule}{mole\ ^oK^2}$ | $T^2\ ^oK^2$ | $\frac{C}{T}$ $\frac{mJoule}{mole\ ^oK^2}$ | $T^2\ ^oK^2$ |
|---|---|---|---|---|---|
| 45.7 | 26.228 | 49.0 | 28.787 | 46.8 | 33.144 |
| 46.4 | 26.691 | 50.5 | 29.309 | 42.3 | 33.791 |
| 46.7 | 27.195 | 51.0 | 30.117 | 42.1 | 34.566 |
| 46.1 | 27.649 | 53.9 | 31.874 | 42.4 | 35.383 |
| 47.5 | 28.221 | 53.4 | 32.419 | 38.7 | 36.195 |
| | | | | 37.3 | 37.139 |

Table A9. Specific heat of $CeRu_2$ 4.0 Koe field

| $\frac{C}{T}$ $\frac{mJoule}{mole\ ^oK^2}$ | $T^2\ ^oK^2$ | $\frac{C}{T}$ $\frac{mJoule}{mole\ ^oK^2}$ | $T^2\ ^oK^2$ | $\frac{C}{T}$ $\frac{mJoule}{mole\ ^oK^2}$ | $T^2\ ^oK^2$ |
|---|---|---|---|---|---|
| 44.9 | 25.742 | 49.3 | 28.723 | 39.8 | 33.026 |
| 46.3 | 26.179 | 49.7 | 29.296 | 40.4 | 33.788 |
| 47.3 | 26.642 | 50.2 | 29.309 | 41.9 | 34.536 |
| 46.3 | 27.200 | 50.3 | 30.476 | 42.9 | 35.306 |
| 47.9 | 27.708 | 44.1 | 31.815 | 38.8 | 36.055 |
| 47.6 | 28.183 | 40.3 | 32.386 | | |

Table A10. Specific heat of $CeRu_2$ 6.0 Koe field

| $\frac{C}{T}$ $\frac{mJoule}{mole\ ^oK^2}$ | $T^2\ ^oK^2$ | $\frac{C}{T}$ $\frac{mJoule}{mole\ ^oK^2}$ | $T^2\ ^oK^2$ | $\frac{C}{T}$ $\frac{mJoule}{mole\ ^oK^2}$ | $T^2\ ^oK^2$ |
|---|---|---|---|---|---|
| 47.1 | 26.865 | 45.8 | 29.805 | 40.5 | 33.092 |
| 48.2 | 27.617 | 39.9 | 30.422 | 42.7 | 33.760 |
| 49.7 | 28.633 | 38.1 | 31.176 | 43.0 | 34.498 |
| 49.0 | 29.303 | 37.4 | 31.721 | | |

Table A11. Specific heat of $CeRu_2$
Sample cooled in 9 Koe field
Sample measured in 9 Koe field

| $\frac{C}{T}$ $\frac{mJoule}{mole\ {}^oK^2}$ | $T^2\ {}^oK^2$ | $\frac{C}{T}$ $\frac{mJoule}{mole\ {}^oK^2}$ | $T^2\ {}^oK^2$ | $\frac{C}{T}$ $\frac{mJoule}{mole\ {}^oK^2}$ | $T^2\ {}^oK^2$ |
|---|---|---|---|---|---|
| 35.0 | 18.009 | 43.2 | 24.785 | 38.0 | 31.118 |
| 35.3 | 18.483 | 43.9 | 25.229 | 38.0 | 31.815 |
| 36.0 | 18.999 | 44.8 | 25.628 | 38.2 | 32.428 |
| 37.9 | 20.677 | 45.4 | 26.079 | 39.5 | 33.047 |
| 38.9 | 21.285 | 46.1 | 27.072 | 40.5 | 33.755 |
| 39.8 | 21.933 | 41.2 | 27.575 | 41.9 | 34.499 |
| 40.0 | 22.457 | 36.3 | 28.095 | 39.3 | 35.257 |
| 41.2 | 22.992 | 35.5 | 28.643 | 37.2 | 36.145 |
| 41.5 | 23.575 | 35.8 | 29.202 | 36.4 | 37.098 |
| 42.1 | 23.985 | 36.1 | 29.826 | 37.2 | 37.862 |
| 43.1 | 24.371 | 37.0 | 30.467 | | |

Table A12. Specific heat of $CeRu_2$
Sample cooled in zero field
Sample measured in 9 Koe field

| $\frac{C}{T}$ $\frac{mJoule}{mole\ {}^oK^2}$ | $T^2\ {}^oK^2$ | $\frac{C}{T}$ $\frac{mJoule}{mole\ {}^oK^2}$ | $T^2\ {}^oK^2$ | $\frac{C}{T}$ $\frac{mJoule}{mole\ {}^oK^2}$ | $T^2\ {}^oK^2$ |
|---|---|---|---|---|---|
| 5.85 | 1.826 | 34.5 | 17.668 | 36.1 | 29.189 |
| 5.81 | 1.956 | 35.2 | 18.268 | 36.6 | 29.810 |
| 6.47 | 2.084 | 36.3 | 18.867 | 37.2 | 30.441 |
| 7.10 | 2.573 | 37.1 | 19.658 | 37.6 | 31.050 |
| 7.22 | 2.592 | 39.0 | 21.364 | 37.8 | 31.678 |
| 8.38 | 2.928 | 40.0 | 22.024 | 38.6 | 32.306 |
| 9.51 | 33.92 | 40.9 | 22.686 | 39.6 | 33.033 |
| 10.5 | 4.042 | 41.8 | 23.375 | 40.2 | 33.767 |
| 11.35 | 4.564 | 42.8 | 24.145 | 41.9 | 34.456 |
| 12.2 | 4.866 | 44.0 | 25.009 | 39.3 | 35.212 |
| 12.8 | 5.171 | 44.9 | 25.656 | 37.2 | 36.037 |
| 14.1 | 5.792 | 45.7 | 26.119 | 37.0 | 36.966 |
| 16.1 | 6.744 | 46.1 | 26.585 | 36.9 | 37.869 |
| 17.8 | 7.550 | 45.9 | 27.078 | 37.5 | 38.699 |
| 19.5 | 8.361 | 41.8 | 27.588 | | |
| 24.2 | 11.546 | 35.6 | 28.645 | | |